UPPSALA
UNIVERSITET

UPTEC F 24005
Examensarbete 30 hp
Februari 2024

Measuring bacterial metabolism and antibiotic susceptibility

using silicone nanowire field-effect transistors.

George Alhoush

Civilingenjör i teknisk fysik

UPPSALA UNIVERSITET

Measuring bacterial metabolism and antibiotic susceptibility using silicone nanowire field-effect transistors.

George Alhoush

Abstract

Antimicrobial resistance is considered by many prominent researcher and scientist as a profound global health crisis that us humans must face in the next decade. It is threatening the effectiveness of these once-reliable weapons against bacterial infections and leaving us susceptible to pathogenic agents. The indiscriminate overprescription of antibiotic in healthcare and animal husbandry, has led to an increased emergence of “super bugs”— a resistant strain of bacteria that were once susceptible to antibiotic—. The escalating creation of those resistant bacteria has been coupled with a proliferation of research papers that seek to explain the working mechanism of antibiotics and their efficacy on the bacterial pathogens, however these efforts often fall short of explaining the impact that antibiotics has on the bacterial metabolism.

This project utilizes an established technology, specifically silicone nano-wire ion-selective field-effect transistor in an innovative approach to discern alteration in the metabolic pathways induced by various antibiotics. The methodology involves measuring extracellular acidity of the tested culture and converting it to an electrical signal to extract valuable information about the metabolic process of the bacteria, and how is altered in the presence of antibiotics.

Empirical observations pertaining bacteriostatic antibiotics suggests comprehensive suppression of metabolic pathways, encompassing the efflux transition from acetyl-CoA to acetate, resulting an elevated pH level in cultures treated with bacteriostatic agents relative to their wild-type counterparts.

Our experimental data also indicates a shift in bacterial metabolic and physiological responses to bactericidal antibiotic-induced stress which include an increased respiration rate, and a heightened activity of the TCA cycle in the test group with bactericidal antibiotics, causing acetate uptake from the medium and decelerating the acidification of the treated culture compared to the wild-type.

The results clearly demonstrate a successful utilization of the chip to further study the effects that antibiotics have on bacteria and the interplay between bacterial metabolism and antibiotic efficacy.

Teknisk-naturvetenskapliga fakulteten

Uppsala universitet, Utgivningsort: Uppsala

Handledare: Yingtao Yu Ämnesgranskare: Zhen Zhang

Examinator: Tomas Nyberg

UPPSALA
UNIVERSITET

Master Thesis in Engineering Physics
30 hp

Author:
George Alhoush

Measuring bacterial metabolism and antibiotic susceptibility using silicon nanowire field-effect transistors

Supervisor:
Yingtao Yu

Subject reader:
Zhen Zhang

Examiner:
Tomas Nyberg

Department of Electrical Engineering - Solid-state electronics

January - May, 2024

1 Populärvetenskaplig sammanfattning

Antibiotikaresistans utgör ett av de värsta problem människor kan stöta på inom de kommande åren. Det kan ha dystopiska påverkan på människors levandssätt och kosta staten massa pengar för att bekämpa det och lindra de negativa effekterna. Det är av yttersta vikt att samhället i stort, och sjukvården i synnerhet, utforskar och implementerar en mångfald av lösningar för att förebygga denna hotfulla framtida verklighet.
Ett sätt för att adressera detta problem innefattar föreskrivning av adekvata antimikrobiella medel för specifika patogener och angivande av korrekta doseringsregimer. Det kräver att läkaren har en viss förkunskap kring de bakterierna som orsakar sjukdomen för att avgöra om dessa bakterier är känsliga mot den valde antibiotikan. Denna information kan åstadkommas genom att utföra vad som kallas "Mikrobiologiska sensitivitetstester", men de verktygen som läkaren har i deras verktygslåda nuförtiden för att genomföra dessa tester bedöms vara bristande och otillräckliga. Det här projektet försöker stödja läkare i deras kamp mot antibiotikaresistens genom att tillverka ett mikrochipp som kan utföra snabb mikrobiologiska sensitivitetsteseter. Det aktuella mikrochippet är konstruerat för att utvärdera antibiotikaresistens hos bakterier genom att mäta den metaboliska aktiviteten och omvandla den till en elektrisk signal.

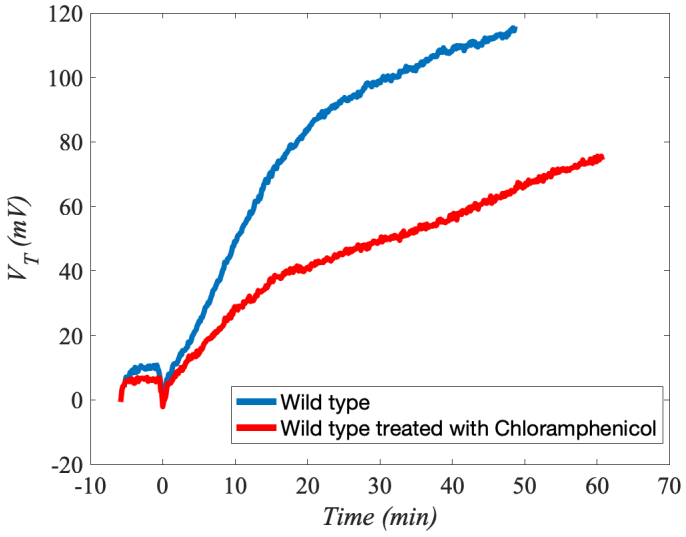

Figure 1.1: En figur som skildrar resultatet för ett experiment

En upphöjd metabolisk aktivitet hos bakterier motsvara en hög elektrisk signal och vice versa. När bakterier dör av antibiotika, då förväntar vi oss en lägre nivå av aktivitet och därmed en lägre signal.
Signalen som visas i Figur1.1 är en elektrisk signal och den beskriver hur bakterier beter sig i frånvaro av antibiotika (Den svarta linjen) och i närvaro av antibiotika (Den röda linjen). Man ser en tydlig skillnad i nivåer av de olika signaler i figuren, och det är ett bevis, att bakterierna som används i detta experiment var känsliga mot Chloramphenicol.
Resultatet i det här projektet ser lovande ut, eftersom chippet kan snabbt detektera om bakterier dör i närvaro av antibiotika och vilka antibiotika är mest effektiva. Det här chippet kan stödja läkaren, och låta de fatta informativa beslut kring behandling som bäst gynnar deras patienter och samhället.

Contents

2 Introduction

Since its discovery, antibiotic has been our first line of defense against bacterial infections in both human and animals. It has saved countless of lives that would otherwise have been killed and helped increasing the life expectancy from 47 in most industrialized country to 78.8 in just under a century [1]. However, due to antibiotic resistance, our antibiotics are gradually losing their effect on today's bacteria [2]. The negative effect of that phenomenon includes millions of injuries and hundreds of thousands of deaths, 55 billion dollars elevation in health care cost and loss of productivity each year, according to the Centers for Disease Control and Prevention (CDC's) estimate [3].
Antimicrobial resistance refers to the phenomenon that microorganisms such as bacteria, viruses or fungi keep growing and dividing even in the presence of medicine which they were susceptible to earlier [3]. Antibiotics resistance is considered to be a subcategory of antimicrobial resistance where the medicine that has been used is antibiotic. Some of the ways microorganisms can follow to achieve resistance are biofilm formation [4], in addition to genetic mutation [5].
One of the main causes of antibiotic resistance is overprescribing or prescribing wrong antibiotic to the bacterial pathogen [6]. It is therefore crucial to effectively determine the right antibiotic with the proper dosage for each patient. This can be achieved by performing an antibiotic susceptibility test (AST) to check antibiotics efficacy against the host's bacteria. The problem facing doctors is that those traditional tests take on average between 12 and 24 hours to get the results back [7] while the patient may be in dire need of antibiotic during that time in the case of serious bacterial infections. Over the last few years, researchers have brought up with different approaches to test antibiotic susceptibility. One example is bacterial metabolic monitoring [8], where the main detection principle depends on measuring the bacterial metabolism to distinguish the resistant strains from the susceptible ones. Another approach is impedance measurement [9], which relies on measuring the variations in resistivity of a solution due to metabolic byproducts caused by cell death or growth stimulated by antibiotics. Due to challenges encountered during the testing phase, none of the above-mentioned technologies has yet to reach clinical utilization.

This project introduces a novel solution to significantly suppress the long AST time, which relies on the ion-selective field-effect transistor (ISFET)

sensors, featuring label-free, real-time, and rapid test. The device is fully CMOS compatible, with low cost, and easy to operate in addition to its high integration capabilities on a silicon chip. Moreover, the detection method is electrical which is highly advantageous due to its accuracy, and efficiency of signal processing.

3 Theory

3.1 Ion-selective field-effect transistor

The ISFET is extremely similar to the metal-oxide-semiconductor field-effect transistor (MOSFET), consisting of source, drain and gate terminals. However the gate bias of the ISFET is provided to the transistor by a reference electrode submerged in an aqueous solution rather than metal wrapping the channel, as shown in Figure 3.1.

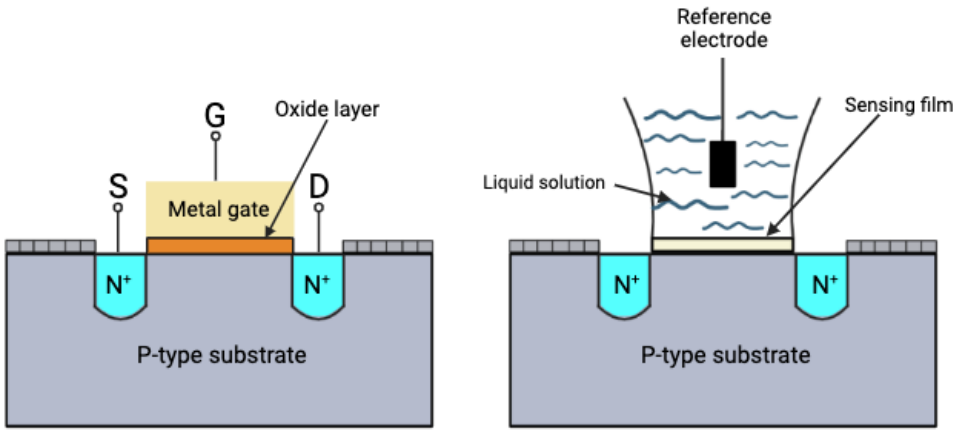

Figure 3.1: A cross-section schematic of the MOSFET to the left and the ISFET to the right

It is therefore not surprising that most papers on this subject describe the theory of the MOSFET, as it applies to both devices with a slight distinction regarding the threshold-voltage V_T.
ISFETs share the foundational architecture inherent to MOSFETs, comprising three pivotal constituents: source, drain, and gate and they can take one of two combinations, either PNP or NPN the characteristic of which depends on the type of main carriers in the channel. An additional sensing film is needed for these devices to work as illustrated in Figure 3.1, which can selectively interact with target analytes. Various materials have been explored and employed as sensing films in ISFET technology. These materials exhibit distinct characteristics, contingent upon the specific molecules or ions earmarked for detection. Among the noteworthy materials are silicon

nitride (Si_3N_4)[10] and silicon oxide (SiO_2)[11]. However, in the context of this project, hafnium oxide (HfO_2) has been judiciously chosen as the designated sensing film for pH sensing. Choosing hafnium-oxide as the device's sensing film is attributed to its high dielectric constant, resulting in a large oxide layer capacitance with 5-nm thickness. Therefore the voltage shared by oxide layer can be greatly reduced, leading to enhanced signal response approaching Nernst level[12].
The general expression for the drain current in both ISFET and MOSFET in the non-saturated region is

$$I_d = C_{ox}\mu\frac{W}{L}[(V_{gs} - V_T)V_{ds} - \frac{1}{2}V_{ds}^2] \tag{3.1}$$

where C_{ox} is the capacitance per unit area for the oxide-layer, μ is the carrier mobility, W, L are gate width and length respectively, while V_{gs} and V_{ds} refers to gate-source voltage and drain-source voltage respectively [13].
The equation for the threshold-voltage on the other hand is different between a MOSFET and an ISFET. The equation for the MOSFET is given by:

$$V_T = \frac{\phi_M - \phi_{si}}{q} - \frac{Q_{ox} + Q_{ss} + Q_B}{C_{ox}} + 2\phi_f \tag{3.2}$$

Where ϕ is the workfunction for the gate metal (ϕ_M) and silicon (ϕ_{si}), while Q is the accumulated charge in the oxide (Q_{ox}), at the oxide-silicon interface (Q_{ss}) and in the depletion region (Q_B) [13].
The equation for the V_T in ISFET is slightly different because the gate voltage is provided by solution biased by a reference electrode and we have to take into account the solution/oxide interface:

$$V_T = E_{ref} - \varphi_s + \chi^{sol} - \frac{\phi_{si}}{q} - \frac{Q_{ox} + Q_{ss} + Q_B}{C_{ox}} + 2\phi_f \tag{3.3}$$

The workfunction for the gate metal(ϕ_M) from the last equation has disappeared in this equation because it is replaced by (E_{ref}) which is the constant potential deliverd by the electrode, while "$\varphi_s + \chi^{sol}$" is a value for a potential measured in volt. To further explain (φ_s) is the surface potential at the solution/oxide interface, and it is shown to be a function of the solution pH while (χ^{sol}) is the surface dipole potential of the solvent and thus has a constant value, Lastly, ϕ_f is the flat band voltage which is also a constant[13].
Drain current is eventually what is been measured during the experiment due

to its higher accuracy and higher resolution compared to measuring voltages. It is therefore vital to understand how drain current is related to the pH level of the aqueous solution.
Figure 3.2 shows the I_d/V_{ds} curve for an ISFET in different pH levels of the aqueous solution, and a constant V_{ref} potential from the electrode. We can clearly see how the drain current changes in value at various pH levels promoting a distinct threshold voltage for the device with each pH level.

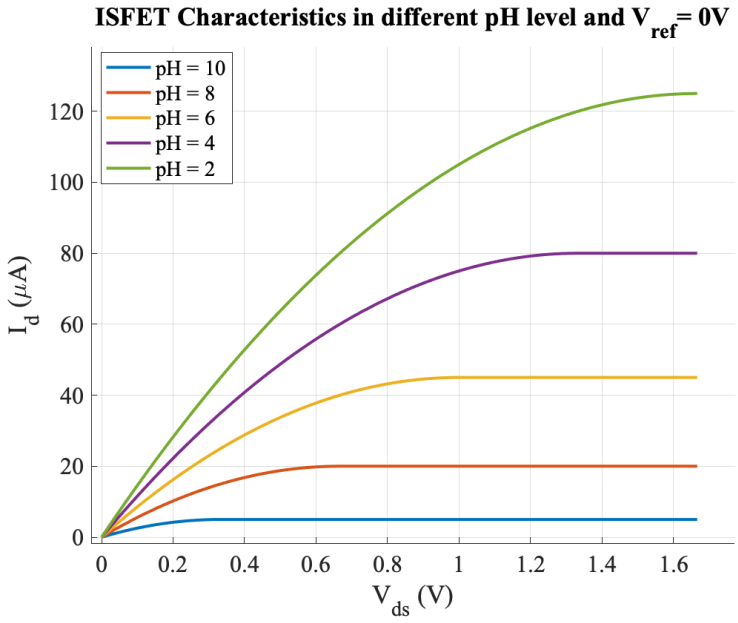

Figure 3.2: I_d/V_{ds} curve in different pH levels.

The measured changes of the ISFET current can be converted to the variation of its threshold voltage, so that it is easy to extrapolate the threshold voltage changes of for each ISFET for the changing pH level induced by bacterial metabolism.

3.1.1 Electrical double layer

Understanding how the drain current and consequently the threshold voltage changes due to pH variations in the solution demands a deeper insight of the concept **Electrical double layer (EDL)**. EDL emerges upon the contact between an oxide-layer and a solution, and it resides at the solid/liquid

interface of the device.

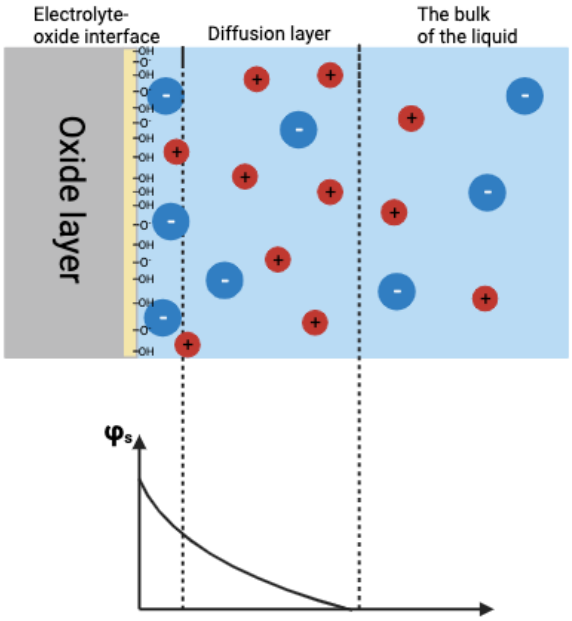

Figure 3.3: An illustration of the EDL with the potential distribution

As evident by Figure 3.3 the OH^- group works as the receptors and donors for the hydrogen ions H^+ according to the following chemical reaction:

$$M - OH \iff M - O^- + H_s^+$$

$$M - OH_2^+ \iff M - OH + H_s^+$$

Where M denotes that these chemical belong to the oxide layer. OH^- group are the ones responsible for the pH response generation, and it is crucial here to identify and differentiate two types of pH:

1. pH_s: The pH level of the liquid at the solid/liquid interface(H_s^+).
2. pH_b: The pH level of the bulk liquid seen to the right of Figure 3.3.

The change to the pH_b level will not be accompanied with an equal change in the pH_s level, as the dynamic equilibrium between H^+ and OH^- will resist

the change creating an intrinsic buffer capacity along the oxide surface (β_{int}) [14]. The change in the surface potential φ_s due to the change in the bulk pH levels generates threshold voltage change of the ISFET as the signal, which can be expressed by the following equation [15]:

$$\begin{aligned} \frac{\partial \varphi_s}{\partial pH_{bulk}} &= -2.3\alpha\frac{kT}{q}, \text{ where} \\ \alpha &= \frac{1}{\frac{2.3kC_{EDL}}{q^2\beta_{int}} + 1} \end{aligned} \tag{3.4}$$

Where k is the Boltzmann's constant, T is the temperature, q is the charge, and C_{EDL} is the double layer capacitance.
It is clear from the equation that the ideal, and the highest response that the device can register due to pH change coincide when $\alpha = 1$, hence β_{int} should be infinite, i.e pH_s should stay constant when pH_b is changing. In this case $\frac{\partial \varphi_s}{\partial pH_{bulk}}$ will become:

$$\frac{\partial \varphi_s}{\partial pH_{bulk}} = -2.3\frac{kT}{q} = 59.2mV \tag{3.5}$$

Which is referred to as the Nernst limit of sensitivity, the highest theoretical response due to pH change [16].

3.2 Silicon nanowire field-effect transistor

Silicon nanowire field-effect transistor (SiNWFET) is a type of ion-selective field-effect transistor (ISFET) in which the active channel is made of a silicon nanowire [17].
This device has experienced a notable surge in interest owing to its exceptional attributes, including high aspect ratio, low power consumption, heightened sensitivity, and selectivity, real-time detection capabilities and fully CMOS compatibility [18].
The focal point of this research revolves around the bonding of silicon nanowires with chemical or biological receptors. The main objective is to exploit the specific binding interactions between these receptors and the target molecular compounds or chemical ions of interest. Upon successful binding events, the silicon nanowires produce an electrical signal, serving as an indication of the presence of the desired target.

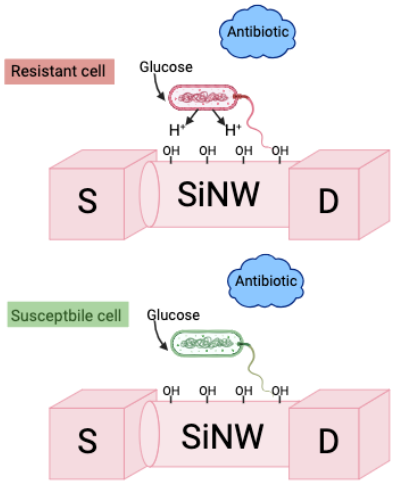

Figure 3.4: An illustration of the SiNWFET during the experiment

By harnessing the unique properties of silicon nanowires and tailoring them with selective receptors, this approach offers high sensitivity and specificity in detecting the target molecules or in the case of this experiment ions. As depicted in Figure 3.4, the observed phenomenon reveals that the presence of resistant bacteria enables continued metabolic activity, leading to the release of hydrogen ions. Consequently, this released hydrogen ion contributes to an increase in the threshold voltage of the device.

3.3 Bacterial metabolism

Bacterial metabolism refers to the process in which the bacteria oxidize glucose and other organic nutrients to generate the energy needed to sustain growth and vital processes happening inside the bacteria such as motility [19]. It is a highly complex process and can take several pathways to achieve the final result. Figure 3.5 shows the different pathways a bacteria can take where each dot represents an organic chemical compound and each line is the chemical reaction that happened to synthesize that compound.

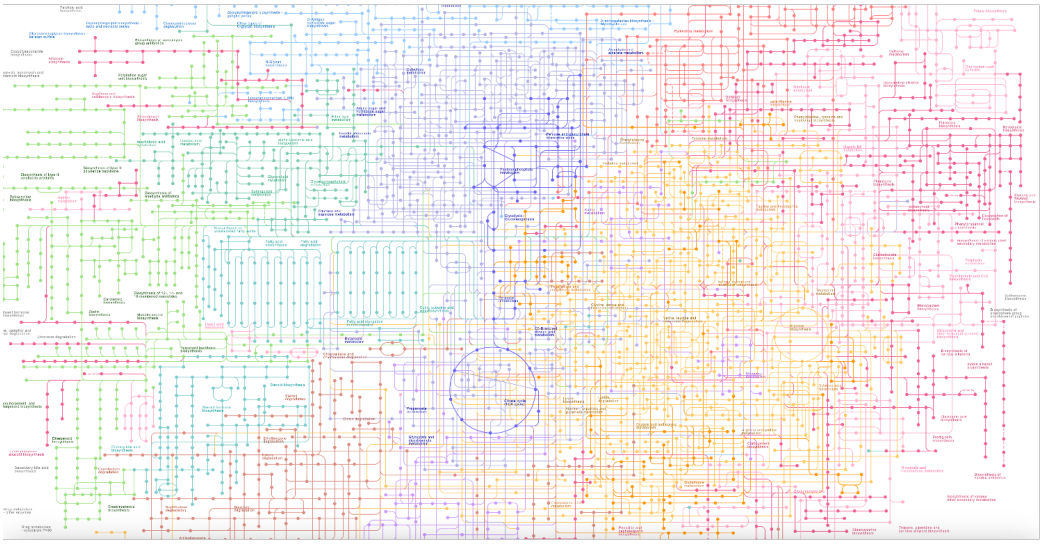

Figure 3.5: The metabolic pathways that a bacteria can take[20]

Due to the high complexity, this report will only focus on glucose metabolism in the presence of oxygen known as respiration, the main metabolic pathway that our experimental bacteria follow as it feeds glucose in Luria-Bertani (LB) broth which acts as a medium for bacterial growth.
The process starts with the Embden–Meyerhof–Parnas (EMP) pathway formally known as glycolysis. This will convert D-glucose ($C_6H_{12}O_6$) into pyruvate ($C_3H_4O_3$) and some ATP according to the following reaction [21].

$$\mathrm{C_6H_{12}O_6 + 2\,ATP + 2\,NAD^+ \longrightarrow C_3H_4O_3 + 4\,ATP + 2\,(NAD(P)H + H^+)}$$

When oxygen is present, Pyruvate will be oxidized to another compound named **acetyl-CoA** which will enter the *tricarboxylic-acid cycle* (TCA) or what is known *Kerbs cycle* which functions oxidatively [22]. Inside the TCA cycle, Acetyl-CoA will be oxidized more in several steps seen in Figure 3.6 producing several ATP and NADH molecules. Finally, the produced NADH will donate two high-energy electrons to the *electron Transport Chain* (check the section on electron transport chain for more information). This entire process is called aerobic respiration and require oxygen to function properly as mentioned earlier.

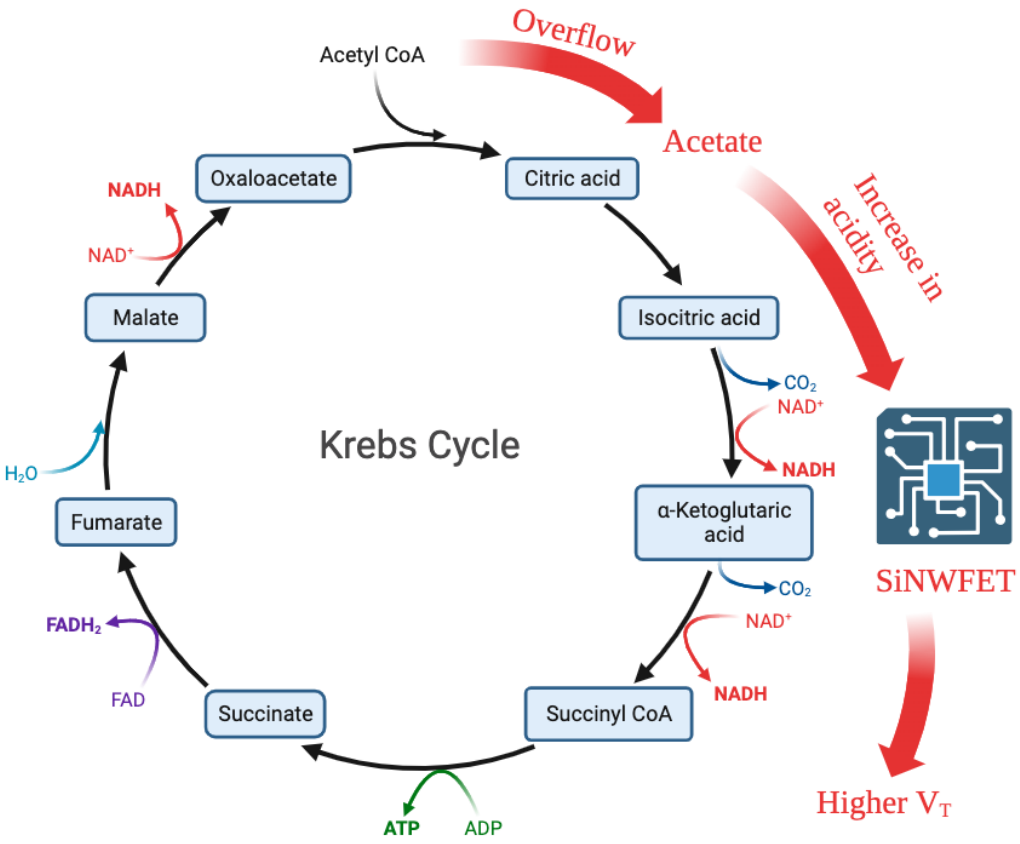

Figure 3.6: The TCA cycle with Acetate overflow

Depending on the level of activity in the TCA cycle, some of the Acetyl-CoA will overflow and synthesis *Acetate* (check Figure 3.6) [23]. The acetate excreted by E. coli is acetic acid, which is a weak acid, and in the case when the entire metabolic process in general, and the overflow from Acetyl-CoA to Acetate in particular is accelerated, then the pH level of the entire LB culture that we are testing will decrease leading to a higher threshold voltage.
This information will be sufficient for the purpose of this project. Further explanation will be provided if needed in the remainder of this report.

3.4 Electron transport chain

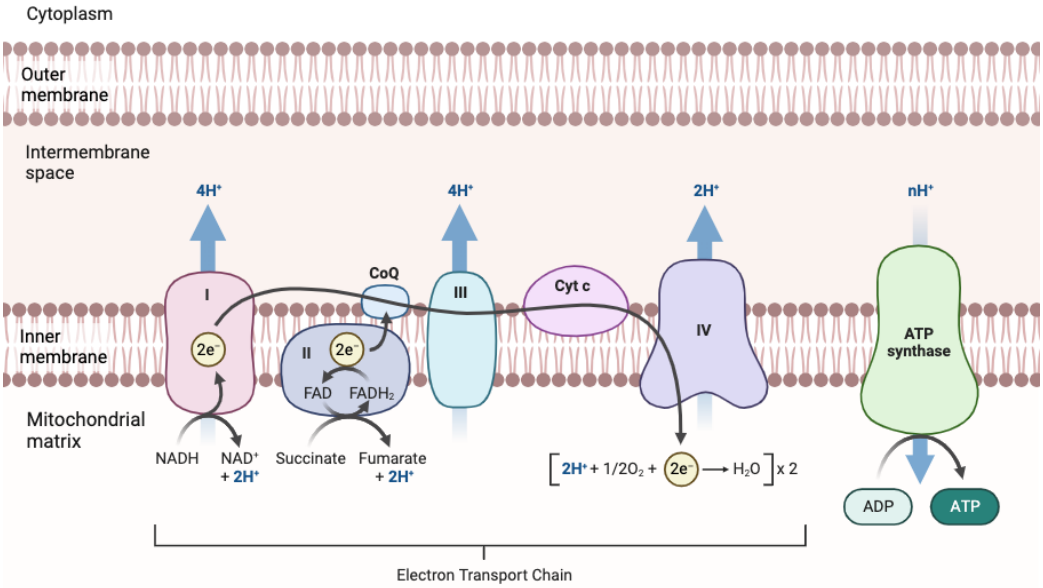

Figure 3.7: An illustration of the ETC with all its complexes and ATP synthase, showing how $NADH$ is oxidised to pump hydrogen ions into the intermembrane space to create a gradient in protons on both sides of the inner membrane, as well as how ATP synthase is using that gradient to generate ATP.

The electron transport chain (ETC) constitutes a sequential arrangement of four protein complexes and an ATP-synthase within the bacterial intermediate membrane. This arrangement allows the flow of the electron through those complexes to maintain a proton gradient across the inner cellular membrane, which drives the rotation of the ATP-synthase and creates new ATP molecules[24]. It is analogous to how electricity is generated by turning a turbine using wind, steam or water.
The ETC proteins in a general order are complex-I, complex-II, complex-III, and complex-IV, with assisted proteins called coenzyme-Q, and cytochrome-C. Compelx-III, -IV and cytochrome-C are not present in *E.coli*, and therefore will not be discussed in this report.

The process is initialized when $NADH$ (donated from glycolysis, and the citric acid cycle) enters complex-I. This $NADH$ molecule is subsequently oxidized inside complex-I into NAD^+ and releases two high-energy electrons into several redox centers inside complex-I with different electron affinity. These differences in affinity level ensure the transfer of electrons from one redox center to the other without skipping any of those redox centers. This reaction is exergonic which means there is a net energy released into complex-I. This energy is consumed by complex-I to inject hydrogen ions from the matrix into the intermembrane space [25].

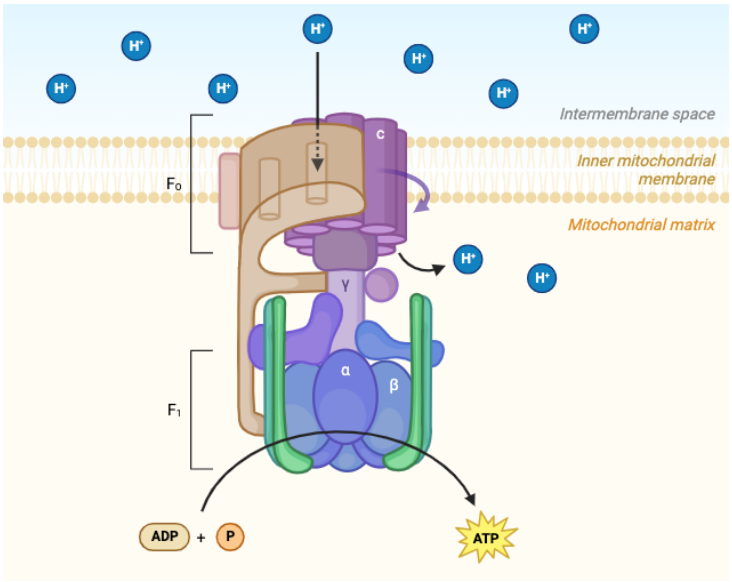

Figure 3.8: An illustration of ATP-synthase

Repeating this process several times will create the gradient along the inner membrane of the cell, establishing the required energy for the proton-motive force. This force will rotate the **C-ring** and subsequently **sub-unit** γ in domain F_0 of the ATP-synthase, creating the required force to synthesize ATP by combining **ADP** and **Phosphate (Pi)** [26]. The chemical reaction to synthesize ATP is called **Phosphorylation**.
Unlike complex-I, complex-II does not pump out hydrogen ions into the intermembrane space of the bacterium. It rather works as a direct link between the electron transport chain and the TCA cycle by directly transferring elec-

trons from succinate to coenzyme-Q, which will help the *E.coli* to coordinate the flow of electrons and metabolic intermediates between the TCA cycle and the ETC [27].

4 Method

This part of the report will explain in detail how the experiment was conducted, alongside the different hardware needed for all the measurements.

4.1 Hardware

4.1.1 The microchip design and fabrication

The chip used in this project has been designed by a fellow researcher (*Yingtao Yu*) within Prof.Zhen's group. However, I actively participated in and closely monitored its entire fabrication process.

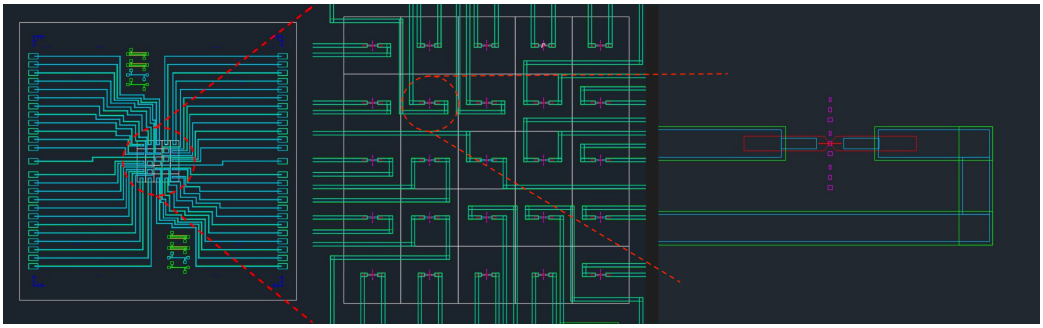

Figure 4.1: The CAD design of the chip with a zoomed view on the SiNWFET devices in the middle.

Autocad was the chosen software to design the schematic of the microchip. Each microchip contains 25 SiNWFET transistors, and the experiment was conduct on several devices in parallel to ensure repeatability and accuracy. Each device consists of a source and a drain wired to contactpads, and a nano-wire which works as the active channel.
Fabricating the microchip follows the approach set by the following thesis [14].
Manufacturing the microchip follows top-down approach, which is fully CMOS compatible and contributes to a better control of the device's dimensions [28]. A 100-mm silicon-on-insulator (SOI) wafer is used to fabricate the SiNWFET devices, where the top layer comprises of 55-nm layer of lightly p-doped silicon above a 145-nm BOX formed by thermal oxidation, while the rest consists of bulk silicon. (check Figure 4.2)

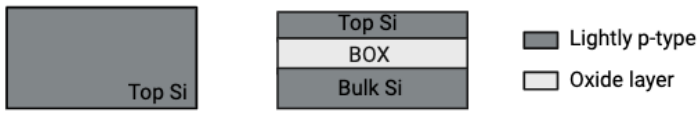

Figure 4.2: A cross section, and a top view of the SOI wafer.

The entire top surface is heavily doped by arsenic implantation to create a n^+ area, while the area where the nano-wire will be constructed is however protected by photoresist mask defined by e-beam lithography (EBL) to keep its p-type characteristic. (check Figure 4.3)

Figure 4.3: A cross section, and a top view of the SOI wafer after arsenic doping.

The source and drain channels are drawn using rapid thermal processing with nitrogen as the activation medium and a temperature of $1000°C$ for 10 second. Subsequently the device structure are defined using combined HSQ and UVN electron beam lithography. (check Figure 4.4)

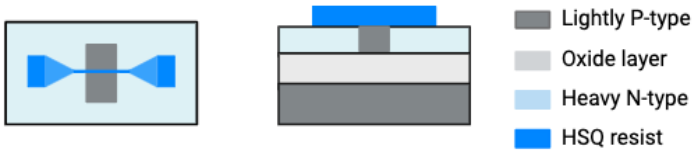

Figure 4.4: A cross section, and a top view of the SOI wafer after drawing and defining the device structure.

In next step reactive-ion etching (RIE) is performed on the entire wafer which will etch the unprotected surface of the wafer to isolate individual devices. (check Figure 4.5)

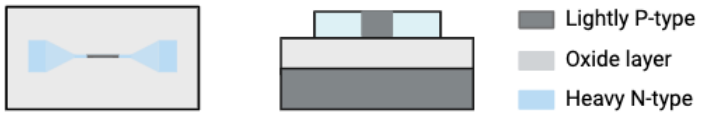

Figure 4.5: A cross section, and a top view of the SOI wafer after RIE.

The heavy n-type layer on the wafer carries a high parasitic resistance. For the device to work properly, this parasitic resistance needs to be reduced. The device also requires constructing ohmic contacts and connecting pads seen in Figure 4.1. This can be accomplished by activating a 10-nm thick layer of nickel silicide (NiSi) using RTP. (check Figure 4.6)

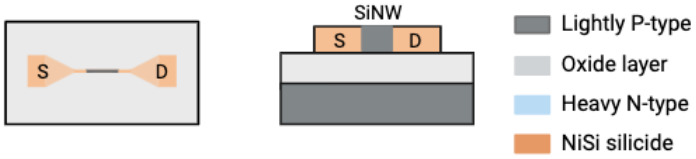

Figure 4.6: A cross section, and a top view of the SOI wafer after activating the NiSi layer.

The last step consists of passivating the top surface with hafnium oxide (HfO_2) to work as a sensing layer for the microchip. A 5-nm layer of HfO_2 is deposited using atomic layer deposition (ALD). (check Figure 4.7)

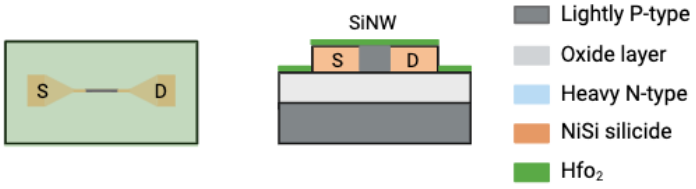

Figure 4.7: A cross section, and a top view of the SOI wafer after HfO_2 passivation.

For more information about manufacturing check [14]. Check Figure 4.8 to see the fabricated chip.

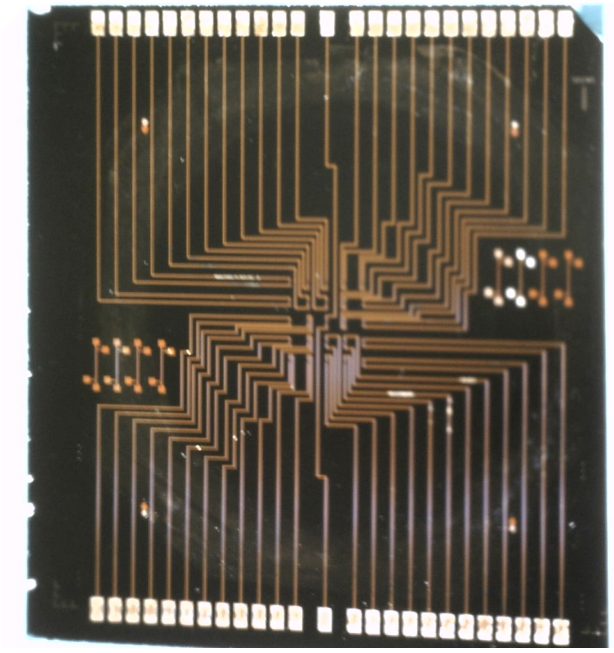

Figure 4.8: An exemplar of the fabricated chip used in the experiments.

4.1.2 Semiconductor Parameter Analyzer (HP4155A)

The Semiconductor Parameter Analyzer (HP4155A) is a laboratory instrument widely used in semiconductor device analysis. Its function is to measure and analyze electrical signals of semiconductor devices, providing researchers with valuable insights into their performance, functionality, and characteristics.
This hardware machine provide researcher with wide and precise tools to realize various electrical measurements, such as current-voltage (IV), capacitance-voltage (CV), and time-domain measurements with high measurement accuracy and broad operating range, making it suitable for characterizing a wide range of semiconductor devices, including diodes, transistors, and integrated circuits.
In this project, we utilized the HP4155A to investigate the electrical properties of semiconductor devices, specifically focusing on silicon nano ISFETs and their IV plots. By employing this device and all its sophisticated tools, we aim to gain comprehensive insights into the behavior and performance of the semiconductor devices under study, contributing to the understanding

and advancement of semiconductor device technology. The data obtained from the HP4155A will be analyzed and interpreted to draw meaningful conclusions and implications for our research objectives.
Overall, the HP4155A plays the largest role in our experimental setup, providing precise and reliable measurements that form the foundation for our comprehensive semiconductor device characterization and analysis.

4.1.3 Switching Unit (Keithley 34970A)

Keithley 34970A is the chosen switching unit to perform this experiment. It is a versatile and a very widely used instrument in the field of electronic testing and measurement. Its data acquisition system is capable of connecting multiple measurement channels to a variety of sensors and devices, and the unit is designed to efficiently switch between different signal sources, making it ideal for applications that require precise and automated data collection from multiple inputs.

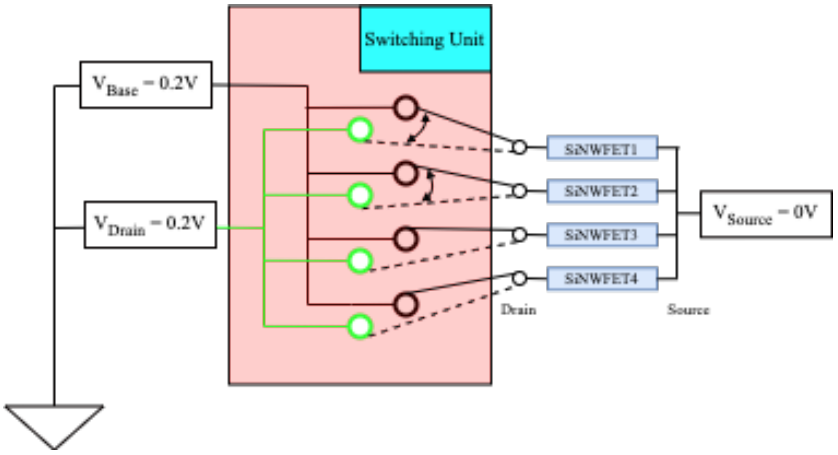

Figure 4.9: Illustration depicting the operational mechanism of a switching unit.

The core functionality of the Keithley 34970A revolves around its capability to route and multiplex signals from a range of sensors, such as temperature sensors, strain gauges, voltage sources, and current sources, among others. This switching capability allows users to sequentially measure multiple channels with a single instrument. Since our experiment measures 4 different

devices simultaneously, the Keithley 34970A will be useful in applying a constant voltage to all four transistor gates while automatically switching the measurement probe from one device to the other. This base voltage will keep all 4 devices in a functional state while the semiconductor parameter analyzer measure the drain current of all 4 devices sequentially, to sufficiently reduce the transient switching current, which is the sub-saturated current flowing in the transistor when it is transitioning between its on and off states.
The instrument comes equipped with various switch modules that can be configured according to specific measurement requirements. These modules can include relay-based switches, solid-state switches, or combinations of both, catering to different voltage, current, and resistance ranges. The Keithley 34970A also provides flexible triggering and scanning options, enabling synchronized measurements and data acquisition at high speeds.
Additionally, the instrument is equipped with various built-in signal conditioning features, such as filtering and amplification, ensuring accurate measurements across a wide range of signal types and amplitudes.

4.1.4 The bacteria sample, and the antibiotics

The bacteria samples used in the experiment were provided by Uppsala University's Biomedical Center. The chip was tested on Escherichia coli (E. coli) K-12 strain as the main pathogenic factor. Pursuant to the praxis, the overnight culture is grown 16 hours before conducting the experiment by adding the fresh LB and inoculating the medium with one single bacterial colony transported from a petri-dish with an inoculation loop, then leaving it on plate shaker at a temperature of 37°C and 200 rpm [29]. A variety of antibiotics, encompassing both bacteriostatic which works by inhibiting bacterial protein synthesis and bactericidal which induce cell death, were administered to the bacterial culture with (33×MIC) concentration. The chosen antibiotics and their dosage are:

- Ampicillin: 2 µL with a concentration 100 µg/ml diluted in water.
- Gentamicin: 2 µL with a concentration 100 µg/ml diluted in water.
- Ciprofloxacin: 2 µL with a concentration 1 µg/ml diluted in water.
- Chloramphenicol: 2 µL with a concentration 250 µg/ml, 125 µg/ml, and 20 µg/ml diluted in ethanol.

The utilization of such high concentration is contributed to the number of cells when calculating the minimum inhibitory concentration. The MIC is derived by performing a killing assay using 5.10^5 cfu/ml [30], while in our experiment the number of cells is approximately 5.10^9 cfu/ml.
Administering two different types of antibiotic will provide valuable analytical data on how the *E.coli* strain reacts in the presence of antibiotics, and reveal the working mechanism of bacteriostatic and bactericidal antibiotic.

4.2 Software

While the core focus of this project centered on hardware aspects, analyzing the experimental data necessitated the utilization of specific software programs, namely Python and Matlab to extract meaningful insights from the experimental data.
As previously delineated, drain current is the parameter subjected to measurement by the device. To determine the threshold voltage, an IV sweep is conducted prior to measuring I_D. A Python file is written to accept the IV sweep and the I_D results as an inputs, and compute the corresponding normalized ΔV_T.
Matlab however is the chosen software program to plots the results of both ΔV_T and the OD600.

4.3 Experiment flow

The experiment was conducted with strict adherence to hygiene practices, ensuring a clean and controlled environment for the study. To maintain high cleanliness standards, the experiment was conducted in Ångström's cleanroom facility.
A bacterial culture containing 200 µL of bacterial suspension was prepared in Eppendorf tubes and incubated on a hotplate at 37°C to mimic the optimal temperature for bacterial growth in the human body. In a separate beaker, a solution of 5 mL of fresh Luria-Bertani (LB) medium with 250 µL of 20% glucose was prepared. The purpose of this setup is to provide a suitable growth environment for the bacteria, as the LB medium provides essential nutrients, and the addition of glucose as a carbon source enhances bacterial growth.
Moving on, the chip and the Polydimethylsiloxane (PDMS) container were meticulously cleaned to eliminate any organic and inorganic residues. Both

the chip and container were sequentially submerged in deionized water (DI water), followed by ethanol, acetone, and isopropyl alcohol. Each submergence step lasted 4-5 minutes. The PDMS container was then carefully placed over the chip, ensuring that it did not interfere the contact pads on the chip. The choice of PDMS as the container material was based on its excellent adhesion with the silicone-oxide layer present on top of the chip. This adhesion is attributed to the chemical compatibility between the two surfaces, which both exhibited hydrophobic characteristics. Subsequently, the assembled chip was placed on a heated chip holder connected to a semiconductor parameter analyzer (HP4155A) for further analysis. check Figure 4.10
50 µL of LB is firstly introduced into the container, along with the reference electrode and a 30 µL of mineral oil to seal the container and prevent LB evaporation. The chip we are using contains 24 ISFETs, but only 4 silicon nano ISFETs are measured simultaneously using the switching unit (Keithley 34970 A). To determine the most suitable ISFETs for further analysis, an IV (current-voltage) sweep is performed on all 24 devices. Subsequently, the four most distinct and representative curves are selected to record the data. The purpose of this selection process is to identify the most responsive and sensitive ISFETs for the specific experimental conditions. By conducting IV sweeps on all 24 devices and carefully choosing the finest four curves, the study ensured the robustness and reliability of the measured data.

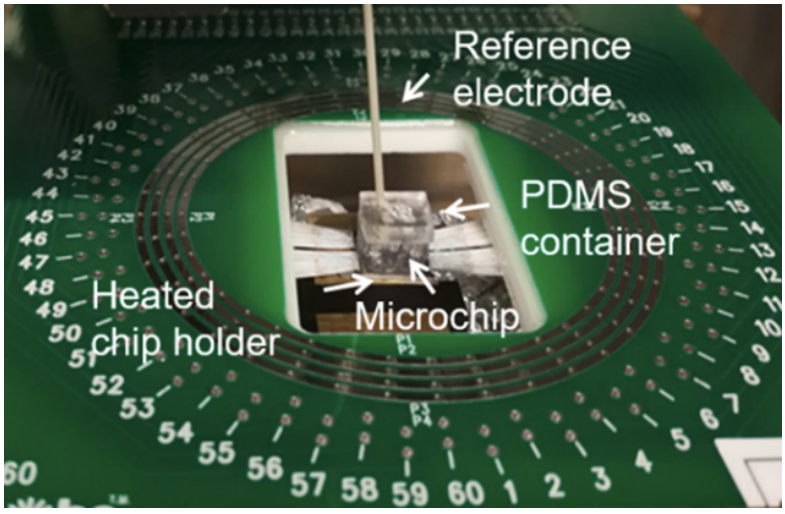

Figure 4.10: The chip on the heated chip holder.

In the meantime, the 200 µL of suspended bacteria are subjected to 1960 relative centrifugal force (RCF) in the centrifuge for 3 minutes facilitating the separation of the bacteria from the previous LB medium used for their cultivation. The supernatant is removed, and subsequently, 133 µL of fresh LB is introduced into the bacterial pellet. In the specific case of measuring the antibiotic group, 2 µL of the chosen antibiotic and concentration is added to the bacterial suspension, followed by a sufficient re-suspension of the entire solution for 10 seconds.
Current sampling is then initiated, and 100 µL of the re-suspended bacteria is added to the container.
The current sweep is conducted for a minimum duration of 3600 seconds (1 hour), during which the data are continuously recorded and saved in a text-file format. The threshold voltages corresponding to the measured drain current are subsequently calculated using a python file which perform the conversion from drain current to threshold voltage by comparing the measured drain current to the IV sweep conducted earlier for each device on the chip. The threshold voltage is then plotted and used for further analysis, as well as studying the effect that each antibiotic has on the bacterial culture.

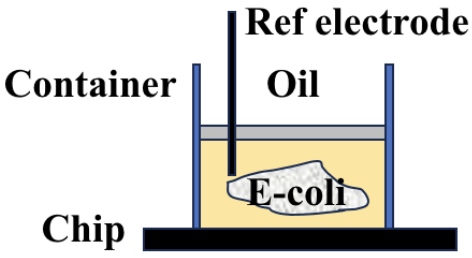

Figure 4.11: An illustration of the chip with the container on top after adding LB, oil, and the studied mutant of the bacteria.

4.4 Optical density measurement

Optical density or OD600 is a measure of the absorption of light by a bacterial culture at the wavelength 600 nm. It is used to estimate the cell concentration in a given liquid culture [31].
Performing the measurement is executed using a bench-top spectrophotome-

ter. The instrument require calibration for the growth medium used in the experiment, which is performed by adding the growth medium without the bacteria to a cuvette and measuring the amount of light absorbed by the medium. This will be used as the reference point for further experiment with the bacteria.
Subsequently, the OD measurement for the bacteria is performed at 10 minutes intervals after adding fresh LB and introducing antibiotics to the bacterial culture.

4.5 Time kill assay

The test require three biological replica of *E.coli* prepared the night before (Check the section on bacteria to see how the overnight culture is prepared), to ensure the repeatability and consistency of the experiment.
Subsequently, on the next day, 1 mL of overnight culture is placed in an Eppendorf tube for each one of the biological replica, and centrifuged for four minutes at a speed of 4000 rpm to separate the bacteria which will precipitate from the supernatant LB. The old LB is be carefully pipeted off, and a new 1 mL of LB with 1% glucose is added to precipitated bacteria and resuspended together to obtain a uniform solution of LB and bacteria. Two Eppendorf tube with 500 µL is aliquoted from the 1 mL solution. The chosen antibiotic is added to one of the tube with the appropriate dosage while the other is left as a control group.

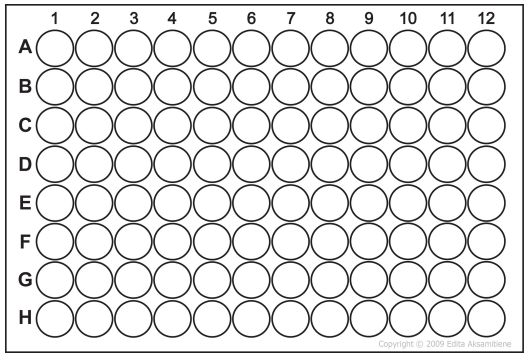

Figure 4.12: 96-well plate

A total volume of 180 µL of Phosphate buffered saline (PBS) is aliquoted

into the wells of a 96-well plate spanning from rows A through F and columns 1 through 7 as depicted in Figure 4.12. Row A and B will be designated for the first biological replica, while the second biological replica will be added to row C and D, and so on. An aliquot of 20 µL of the treated group is dispensed to A1, and an equivalent volume of the control group is administered into well B1. This process should be repeated for the second and the third biological replica from C1 to F1. A subsequent of 6 serial dilution should be performed on the bacterial culture by pipeting up 20 µL of solution from the first column and transferring it to the the second column.(Check Fig. 4.13)

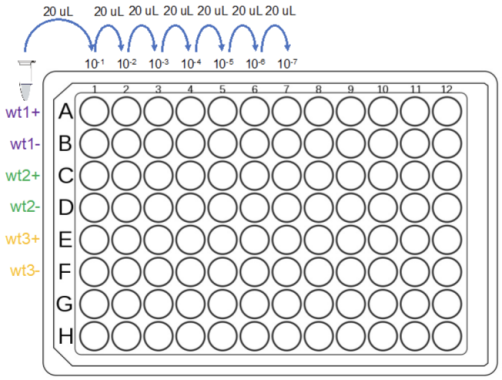

Figure 4.13: Serial dilution in the 96-well plate

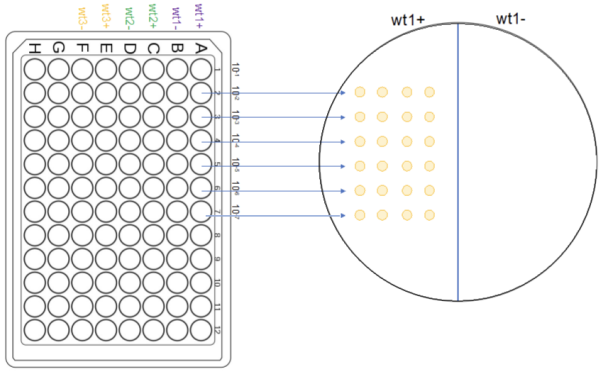

Figure 4.14: Adding the bacteria to an LB agar plate

Lastly, a 10 µL aliquot form each well in row A, column 2 through 7 is pipeted out and transferred onto an LB agar plate arranging it to form four discrete columns, with each column receiving a volume of 2.5 µL. The same process is repeated for all rows. (check Fig. 4.14).
This protocol should be iteratively executed several time over the course of one hour one hour. The number of samples are to be determined based on the required resolution of temporal data.
On the next day, the number of colony formed on the agar plate should be counted. The efficacy and lethality of the chosen antibiotic can be determined, by comparing the number of colonies formed in the treated group and the wild-type.

5 Results and Discussion

This part of the report will present the results obtained from the main experiment, as well as the OD600 measurements for each antibiotic. We will also discuss, and provide a reasonable explanation for the results, by explaining how each of the antibiotic effects the bacterial culture, and more specifically how they affect the pH level of the culture.

5.1 The sensor's principle of detection

The sensing transistor device on the chip can measure the metabolic activity of the bacteria in the solution by monitoring the change in pH level, which is expressed as a change in the threshold voltage (ΔV_T) of the transistor. This change in pH is appertaining to bacterial metabolic activities which excrete organic acids into the medium as a byproduct of that process, leading to an elevated extracellular acidification rate [19]. As introduced in the metabolism section, the presence of these hydrogen ions is ascribed to the overflow of acetate from the tricarboxylic acid (TCA) cycle, when the bacteria experience an inactive metabolic rate.
An alternative explanation for the observed shift in the threshold voltage may be attributed to the introduction of bactericidal antibiotics into the culture. This action could induce cell lysis in a subset of bacterial cells, which consequently will diminish the population capable of metabolizing the carbon source.
The tests were performed on wild-type Escherichia coli (*E.coli*) with several antibiotics, where the bacteria was injected with a high dose of antibiotic, higher than the minimum inhibitory concentration namely 33×MIC to inhibit proliferation of the bacteria and kill them.
The graph of ΔV_T over time with antibiotics is compared to a control group without antibiotics to see when V_T drops marking a decrease in acid excretion and/or indicating bacterial death.

5.2 Treatment with Ampicillin

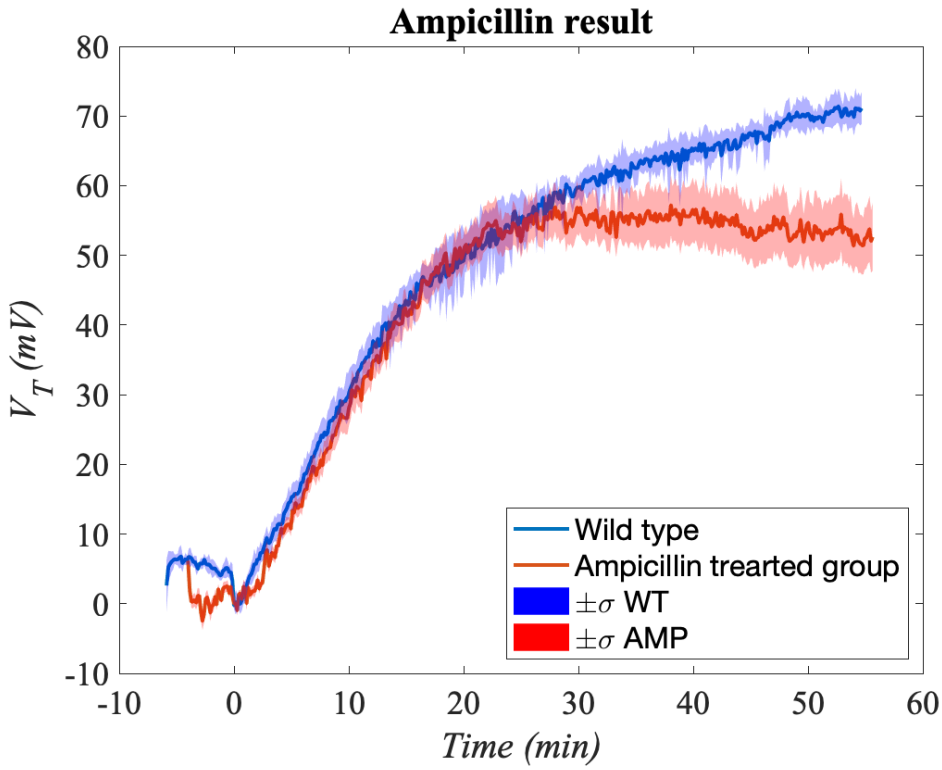

Figure 5.1: ΔV_T vs time curve for ampicillin.

As evident from Figure 5.1, the effect from Ampicillin become apparent after 20 minutes, where we can observe a downward trend in the red line corresponding to the Ampicillin treated culture group, signifying an augmented alkalization of the culture medium.
Ampicillin belongs to semi-synthetic β-lactam bactericidal antibiotic, working by inhibiting bacterial wall synthesis. It is achieved by interfering with the final stages of peptidoglycan synthesis, a crucial component of the bacterial cell wall, and attaching to penicillin-binding proteins to prevent cross-linking of peptidoglycan chains [32]. It was also shown by *P. Belenky* [33], that antibiotic such as Ampicillin induces complex set of metabolic changes in bacteria, mainly accelerating the TCA cycle and creating poisonous molecules called reactive oxygen species (ROS), which induces ROS stress response in

the bacteria. The method of detoxification generally includes an accelerated TCA cycle to dispose the excess ROS, leading the bacteria to a self destructive spiral of accelerated TCA cycle and creating new ROS molecules [34].

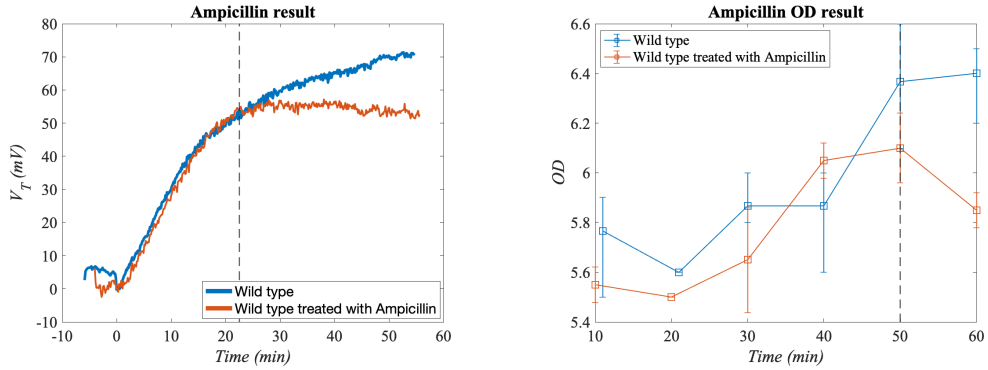

(a) ΔV_T vs time curve for Ampicillin.

(b) OD results for Ampicillin.

Figure 5.2: A comparison between the ΔV_T vs time curve and the OD measurements which indicates a metabolic pathway shift starting at 22 minute after the experiment start and ending with cell lysis at 50 minute.

Inhibiting cell wall synthesis can lead to a disruption in the cellular integrity and a rupture in the cellar barrier, resulting in cell lysis, and subsequently cytoplasmic leakage. This phenomenon prompts the alkalization of the culture medium. Simultaneously the accelerated TCA cycle can decrease and in some instances, entirely inhibit and even reverse the acetate overflow process seen in Figure 3.6 which also has a similar impact on the pH level of the culture.
To ascertain the primary mechanism responsible for the drop in the ΔV_T due to the heightened alkalization of the culture shown in Figure 5.2(a), an OD600 measurement is conducted on the bacteria after introducing 2 µL of 100 mg/mL ampicillin to the culture the same concentration utilized for measuring ΔV_T. The results presented in Figure 5.2(b) indicate a continuous growth for the treated group, following a growth rate akin to the wild-type until a decline is observed after 50 minutes, attributed to cell lysis. However, in the results from the threshold voltage experiment, the drop in ΔV_T induced by the increase in the pH level is evident after only 20 minutes. This temporal mismatch between the two experiments indicates an altered metabolic state,

where the respiration rate is heightened, necessitating an increased influx of acetyl-coA into the TCA cycle, which consequently reverses the acetate overflow process and amplify the alkalization of the culture. The heightened respiration rate is consistent with what has been reported by *Lorbitz.*[35].

5.2.1 Treating $\Delta atpA$ mutants with ampicillin

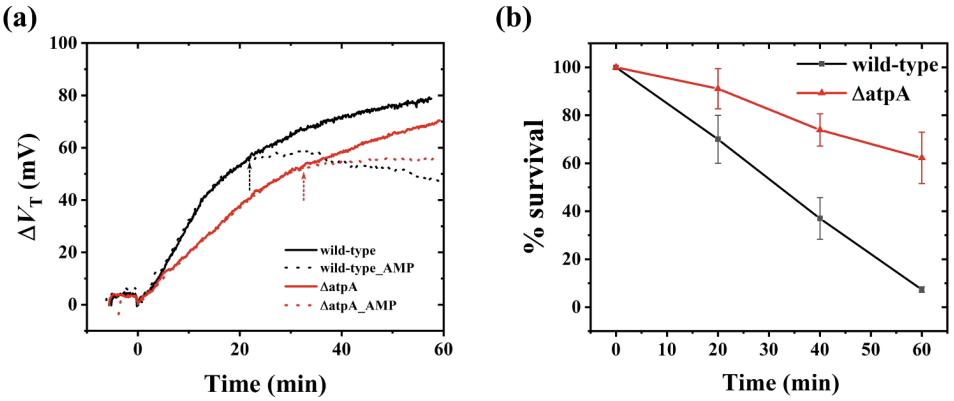

Figure 5.3: (a) .ΔV_T vs. time curves, and (b) time-killing kinetics for wild-type *E.coli* and $\Delta atpA$ mutant, with 100 µg/mL AMP.

To further examine the relation between bacterial metabolic activity and the lethality of ampicillin, an analogous experimental protocol was implemented using an identical concentration of the antibiotic on an $\Delta atpA$ mutant strain of *E.coli*.
atpA gene encodes the enzyme that facilitates ATP synthesis from ADP in the electron transport chain. Consequently the ratio ATP/ADP is expected to be much lower in $\Delta atpA$ mutants where the gene is absent relative to the wild-type resulting in an acidification profile lower than the wild-type as seen in Figure 5.3(a). The rationale behind this observation is the attenuated metabolic activity within the mutant strain, a consequence of the shortage in ATP molecules, the main energy carriers inside the cell.
The bactericidal efficacy of the ampicillin is obsereved to be negatively impacted in the $\Delta atpA$ mutants compared to the wild-type as evidenced by the time kill assay result presented in Figure 5.3(b). This outcome further underscore the importance of metabolic activity for the efficacy of ampicillin, as it diminishes in bacteria cells with significantly reduced metabolic.

5.3 Treatment with Gentamicin

Gentamicin is a β-lactam bactericidal aminoglycoside antibiotic, that functions through inhibition of protein synthesis. Its mechanism for achieving this is through entering the bacteria in an oxygen-dependent active transport, and binding to the 30S ribosomal subunit in bacteria, specifically interacting with the 16S rRNA, resulting in a disruption of the initiation complex formation during protein synthesis leads to the production of incomplete or nonfunctional proteins within the bacterial cell [36].

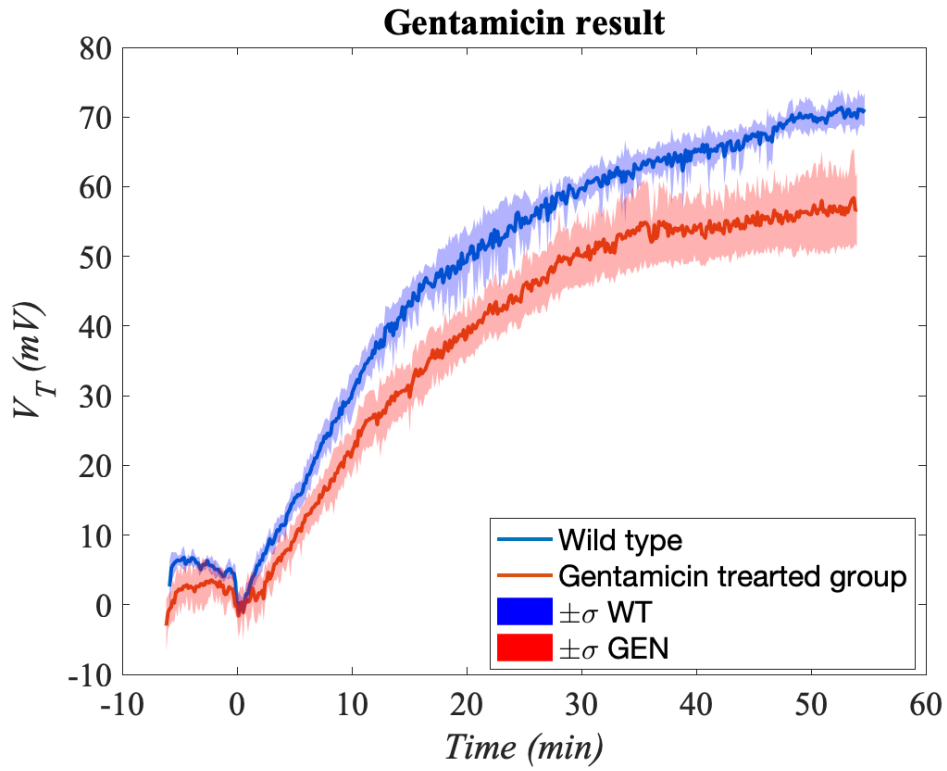

Figure 5.4: ΔV_T vs time curve for Gentamicin.

Gentamicin primary effects gram-negative aerobic bacteria such as *E.coli* because it requires oxygen to passes through the membrane, and is considered a broad spectrum antibiotic [37].
Contradictory to the effect of Ampicillin, the drop in threshold voltage induced by Gentamicin manifested in Figure 5.4 is instantaneous, marking an

attenuated acidification of the culture. The reduction in acidification rate manifested as a reduction in ΔV_T is observable throughout the entire duration of the testing period, reaching the plateau phase after 50 minutes where the disparity in threshold voltage between the wild-type and the treated group stabilizes at approximately -20mV.

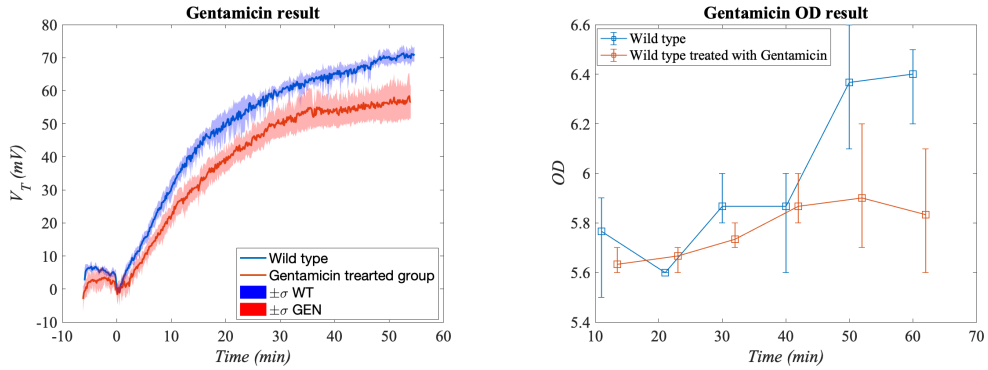

(a) ΔV_T vs time curve for Gentamicin. (b) OD results for Gentamicin.

Figure 5.5: A comparison between the ΔV_T vs time curve and the OD measurements which indicates an elevated respiration rate and cell lysis.

The results from OD600 shown in Figure 5.5(b) is similar to that of Ampicillin. The cell concentration of the treated group is akin to the wild-type for the first 40 minutes. However, the growth rate of the wild-type group is sustained after the 40 minutes mark, while a reduction in the cell concentration for the treated group is observed indicating cell death. The decline in the threshold voltage ΔV_T demonstrated in Figure 5.5(a) is however immediate and persists throughout the entire duration of the testing period which implies an altered and more specifically an accelerated respiration rate in the bacteria. Such acceleration demands an increased influx of acetyl-CoA into the TCA cycle and consequently reversing the overflow mechanism from acetate to acetyl-CoA to provide the necessary resources for the heightened activity in the TCA cycle. This increased influx of acetyl-CoA into the TCA cycle and the reversal of the overflow mechanism deprive the culture of some of its acidic molecules prompting the reduction in the rate of change in the culture pH level compared to wild type, which consequently decreases the ΔV_T of the tested transistors.
A Seahorse XF measurement is a test that micro-biology researchers use to

quantify the oxygen consumption rate(OCR), the flux of oxygen, and extracellular acidification rate(ECAR) in a bacterial culture[38]. The results of the Seahorse XF measurement conducted by researchers in *Lobritz*[35] found an immediate increase in OCR of the tested bacteria after introducing Gentamicin to the culture. This heightened rate of oxygen consumption in the bacterial culture is indicative to the increase in respiration rate induced by Gentamicin and explain the immediate inhibition in ΔV_T. The test results also explain the disparity in temporal efficacy between Ampicillin and Gentamicin. It is attributed to a faster OCR in the culture treated with Gentamicin compared to those exposed to Ampicillin.

5.4 Treatment with Ciprofloxacin

Ciprofloxacin is a fluoroquinolone bactericidal antibiotics. It belongs to a family of broad spectrum antibiotics which are used to treat respiratory and urinary tract infections, and is mostly potent and effective against gram-negative bacilli bacteria such as Escherichia coli and Salmonella spp[39].
The working mechanism of Ciprofloxacin include binding and inhibiting the activity of DNA gyrase and topoisomerase IV, two enzymes responsible for the supercoiling and relaxation of DNA during replication. The interference with the DNA core functionality induces double-stranded breaks in the bacterial DNA leading to the inhibition of DNA replication and transcription process, necessary for protein synthesis[40]. The cumulative effect of DNA damage and inhibition of essential cellular processes leads to the bactericidal action of Ciprofloxacin, causing bacterial cell death. It has also been shown that treating *E.coli* with Ciprofloxacin or other antibiotic in the fluoroquinolone family can generate hydroxyl radicals, and superoxide anions, reactive oxygen species molecules which will contribute to the cell lethality of the antibiotic[41] [42].
It is worth noting, that fluoroquinolone antibiotics are biphasic, which mean the lethality and efficacy of the drugs keeps increasing to a certain concentration known as the optimal bactericidal concentration (OBC). Adding higher concentration than OBC will decrease the efficacy due to the inhibition of RNA synthesis which is required for the bactericidal activity of the drug[43].
The concentration employed in the experiment resides within the ascending phase of efficacy and bactericidal activity but falls short of achieving the OBC for Ciprofloxacin which has been measured to be between 1.2 and 3 µL/mL for *E.coli* in LB medium[44].

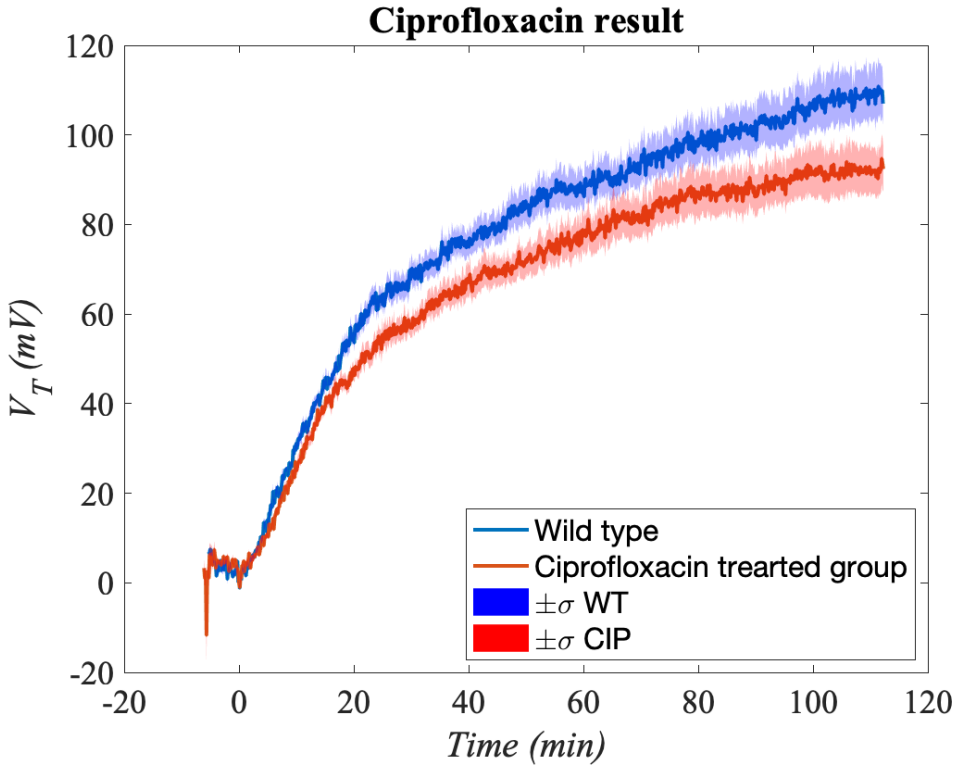

Figure 5.6: ΔV_T vs time curve for Ciprofloxacin.

For the initial 15 minutes, the slope of ΔV_T for the treated group closely mirrors that of the wild-type as clearly indicated in Figure 5.6. Subsequently, the trajectory of the treated group diverges from that of the wild-type after the initial 15 minutes indicating a slower rate of reduction in the pH level of the culture compared to the wild-type. The outcomes of the results from the bacterial culture after introduction of Ciprofloxacin exhibit disparities compared to those observed with the introduction of Ampicillin and Gentamicin. The slope for the bacteria that have been treated with Ampicillin has a positive value at the early stages of the experiment before it reaches a plateau phase followed with a decline and a negative slope. Compared to Ampicillin, the slope of the graph for both Gentamicin and Ciprofloxacin experiences similar behavior at the beginning but do not manifest any decrement at the end but rather stabilizes and converges towards the plateau phase. The sole distinctions however between Gentamicin and Ciprofloxacin resides in the temporal efficacy. As shown in Figures 5.4&5.6, Gentamicin has a shorter

response time than Ciprofloxacin. It also manifests a greater alkalization of the bacterial culture than that induced by Ciprofloxacin.

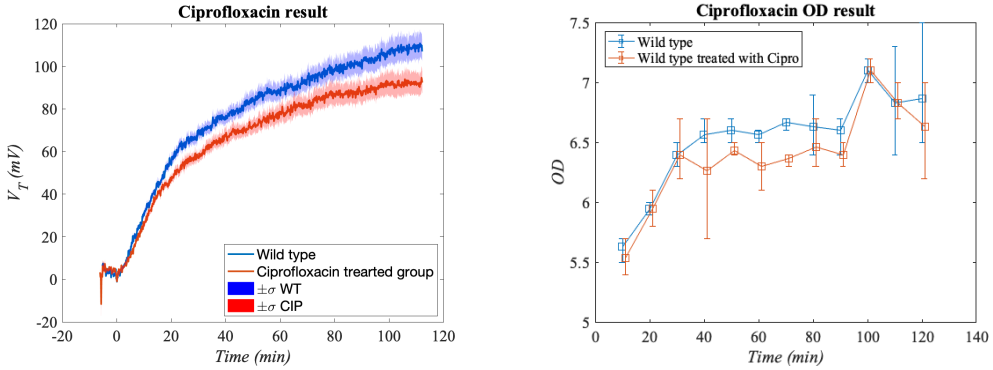

(a) ΔV_T vs time curve for Ciprofloxacin.

(b) OD results for Ciprofloxacin.

Figure 5.7: A comparison between the ΔV_T vs time curve and the OD measurements which shows a slight decrease in respiration rate in comparison to the wild-type.

The outcomes of the OD600 measurements conducted at 10 minutes intervals subsequent to introducing Ciprofloxacin is illustrated in Figure 5.7(b) juxtaposed against the untreated wild-type bacteria. The depicted trajectories of the two datasets demonstrate a convergence, with comparable levels observed within the designated margin of error indicating negative signs of cell lysis within the treated group. Nevertheless, a discernible reduction in threshold voltage for the treated bacterial culture is measurable after 15 minutes. This reduction is attributed to a rise in respiration rate of the bacterial culture which prompts an increase influx of acetate to the TCA cycle. Depriving the culture of some of its acidic molecules will decelerate the acidification rate compared to wild type resulting in a lower ΔV_T in accordance with the working mechanism of SiNWFET transistors. The Seahorse XF measurement performed by *Smirnova* [45] provide an evidence to the statement aforementioned. The researcher in that paper were able to register an accelerated decrease in the level of the dissolved oxygen in LB needed to perform aerobics metabolism signaling heightened metabolic activity, mainly an accelerated TCA cycle. This conclusion is also consistent with the working mechanism of ciporfloxacin as it primarily inhibit protein synthesis in the

bacteria, unlike Ampicillin where the lethality originate from the complex metabolic shifts inside the bacteria.

5.5 Treatment with Chloramphenicol

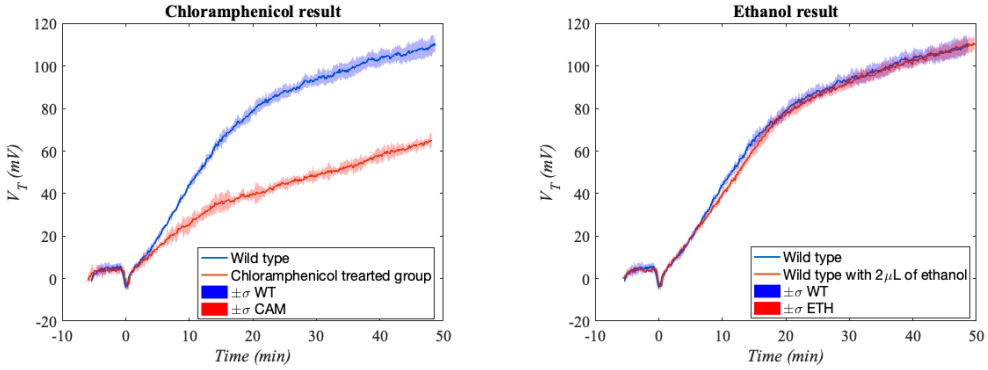

(a) ΔV_T vs time curve for Chloramphenicol.

(b) ΔV_T vs time curve when adding 2 µL of ethanol

Figure 5.8: A comparison between the ΔV_T vs time curve for the treated group with Chloramphenicol and ethanol

Chloramphenicol is one of the broadest antibiotics that human have used. It is potent against gram-positive, gram-negative, aerobic and anaerobic bacteria[46]. Due to its undesirable side effects, the usage of this antibiotic is rare in the present day, however it is still been used to treat eye infections, otitis externa (inflammation of the internal ear canal) and can be used against riskier diseases such as typhoid[47], and cholera[48]. Chloramphenicol is generally considered a bacteriostatic antibiotic, but can exhibit bactericidal behaviors in high concentrations.
Chloramphenicol acts by reversibly binding to the 50S subunit of the 70S bacterial ribosome causing protein synthesis inhibition through obstructing the peptide bond formation[49]. The efficacy of this antibiotic is attributed to its high lipid solubility which facilitates the rapid absorption of the antibiotic into the bacteria and enhances the permeation across diverse tissue types[50].

The threshold voltage ΔV_T exhibits sharp reduction following the introduction of Chloramphenicol and retain this decline throughout the entire

testing phase, distinctly contrasting with the threshold voltage levels reached by the wild-type group as illustrated in Figure 5.8(a). In accordance with the previously expounded theory pertaining ISFET, the observed reduction is indicative of an elevated pH level in the treated culture compared to the untreated wild-type.

It is crucial to note the poor water solubility of Chloramphenicol. Therefor for this experiment, the used samples of Chloramphenicol were dissolved in 97% ethanol to facilitate their use and application. However, due to ethanol's ability to disrupt the bacterial cell membrane and denature its proteins by disrupting their three-dimensional structure, it is considered very effective against bacteria and have bactericidal properties, which establish its efficacy to be used as a disinfectant and antiseptic substance in healthcare sector[51]. To ascertain whether ethanol is responsible for the reduction seen in Figure 5.8(a), an identical experiment was performed after adding 2 µL of 97% ethanol and the results are shown in Figure 5.8(b). The slope of ΔV_T closely resemble that of the wild-type, leading to the inference that at this concentration, ethanol does not contribute to the decrease in threshold voltage,which confirms that the decline in V_T is induced by Chloramphenicol.

The recorded findings after introducing Chloramphenicol to the bacterial sample were unexpected and surprising. According to published research[35], [45], [52], bacteriostatic antibiotics in general and Chloramphenicol in particular has an adverse effect on the bacterial oxygen consumption rate (OCR). Bacterial colonies subjected to bacteriostatic antibiotics like Chloramphenicol experience a reduction in the amount of consumed oxygen which denotes a decline in the respiration rate of the bacteria, which is extended to the TCA cycle of the bacterial cell. A decline in the TCA cycle activity will activate the metabolic overflow process, converting acetyl-CoA to acetate and resulting in the accumulation of this acidic byproduct of metabolism in the tested medium which could lower the pH of the culture and increasing the extracellular acidification rate. Pursuant to the principles underlying ISFET transistors functionality, the threshold voltage is expected to increase when the medium become more acidic, consequently, the anticipated behavior of the threshold voltage after introducing Chloramphenicol was projected to exhibit escalation rather than the observed diminishment, as depicted in Figure 5.9(a).

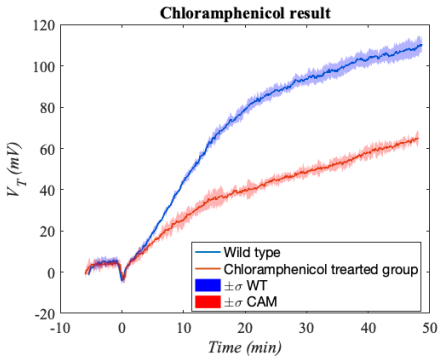

(a) ΔV_T vs time curve for Chloramphenicol.

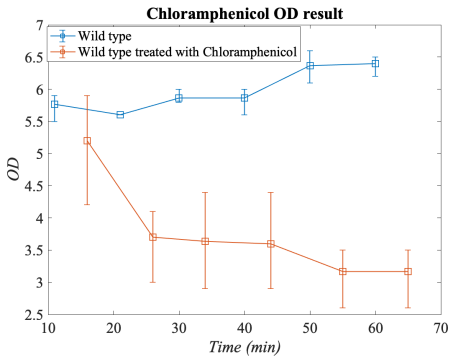

(b) OD results for Chloramphenicol.

Figure 5.9: A comparison between the ΔV_T vs time curve and the OD measurements which shows a fast and noticeable cell lysis with antibiotic concentration of 125 µg/mL.

To elucidate the cause behind the remarkable decline recorded in the Chloramphenicol treated group, a thorough investigation was undertaken, starting with performing OD600 measurement at 10 minutes intervals after introducing Chloramphenicol to the bacterial culture. The results for the OD600 measurement in Figure 5.9(b) illustrate a rapid and sustained decline in the optical density of the bacterial culture, which suggests a concurrent reduction in the colony forming unit per milliliter (CFU/mL), reflecting a decline in cell density or size within the culture due to cell lysis.
It is imperative to underscore that, within this report context, cell lysis pertains to the bacterial cells that have experienced a loss of cellular integrity to such an extent that they become undetectable by the spectrophotometer following antibiotic treatment. These particular bacterial cells are no longer viable and are henceforth considered killed, as a result of the chosen antibiotic's potency.
Since Chloramphenicol falls under the category of bacteriostatic antibiotics, which restrain bacterial growth by inhibiting protein synthesis or interfering with DNA replication without inducing cell death, the findings from the OD600 measurement are deemed inconsistent with the working mechanism and the anticipated effects of bacteriostatic antibiotics.

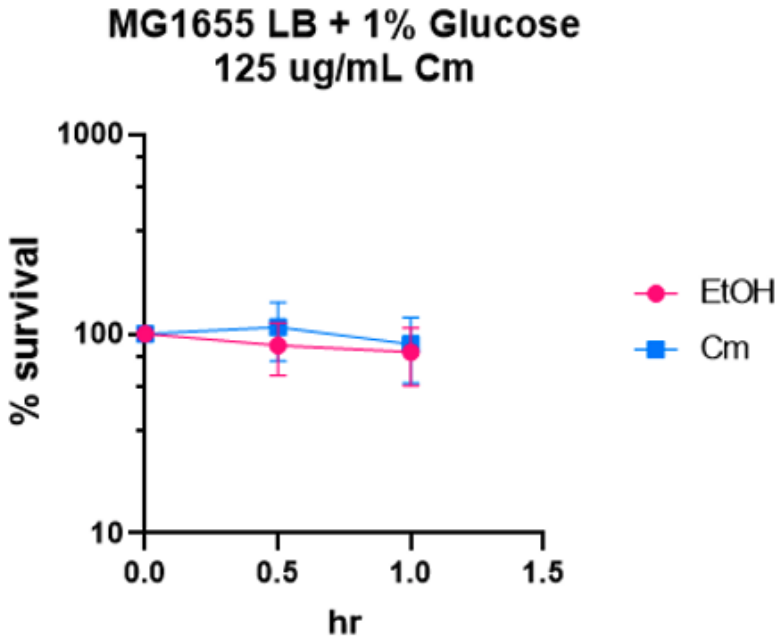

Figure 5.10: Results from the time kill assay conducted for 1 hour, using a concentration of 125 µg/mL.

To reconcile the disparities between the empirical observations and the theoretical underpinnings regarding the efficacy of bacteriostatic antibiotics, a time kill assay was performed to analyze the survival rate of the bacterial group treated with Chloramphenicol. The test was conducted on two groups, one with only ethanol and one with Chloramphenicol dissolved in ethanol. The outcomes derived from the time kill assay is unsurprisingly consistent with the theoretical knowledge of bacteriostatic antibiotic, whereby ethanol did not demonstrate any discernible reduction in the survival rate of the bacterial culture. The rate of survival for the treated group remained at around 100% after 60 minutes, signaling the survival of all the bacteria cells inside the culture, which is inconsistent with the results from the optical density measurements.
The empirical data derived from both the time kill assay and optical density measurements collectively furnish compelling evidence that elucidates the underlying rationale for the sustained decrement observed in threshold voltage in Figure 5.8. In light of the absence of observed cell lysis in the

time kill assay and the documented reduction in OD600 results, a deductive inference can be drawn positing a morphological alteration in cellular form characterized by a diminution in size. Additionally, it is conceivable that Chloramphenicol exerts a dual inhibitory effect on both the TCA cycle and the overflow process, which subsequently diminish the production of acidic byproducts. This concurrent modulation is postulated to result in a discernible reduction in ΔV_T of the subjected transistors.
To further analyze the bacteriostatic effect of Chloramphenicol, two additional concentration were empirically evaluated by subjecting them to identical experimental protocols as applied in the initial evaluation at 125 µg/mL. The two new concentrations are 250 µg/mL representing an increased dosage, and 20 µg/mL, constituting a reduced dosage. These experiments facilitate a comparative analysis of Chloramphenicol's bacteriostatic activity across a range of concentrations.

Treatment with 20 µg/mL Chloramphenicol

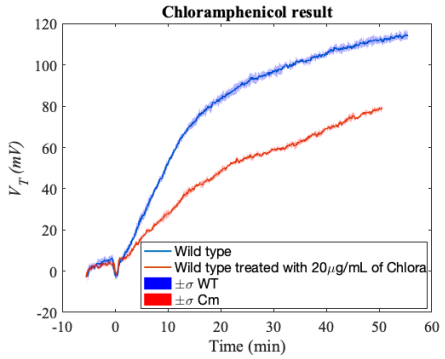

(a) ΔV_T vs time curve for 20 µg/mL of Chloramphenicol.

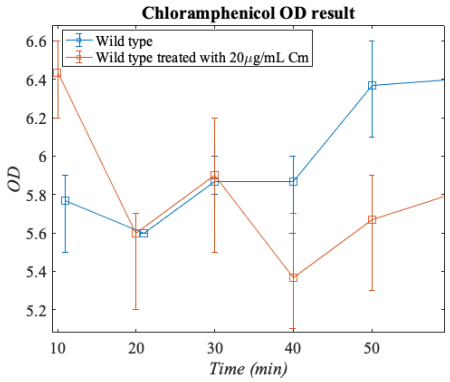

(b) OD results for 20 µg/mL of Chloramphenicol.

Figure 5.11: A comparison between the ΔV_T vs time curve and the OD measurements showing no substantial decrease in cell concentration with antibiotic concentration of 20 µg/mL..

Recent studies have demonstrated that at a concentration of 20 µg/mL, Chloramphenicol exhibit bacteriostatic properties [45] [53] [54]. Its efficacy and potency originates from its ability to inhibit protein synthesis inside the

bacterial cell, and consequently, preventing bacterial growth, thereby prohibiting the proliferation of the bacteria without directly inducing bacterial cell death.
The result from the electrical experiment with the SiNWFET chip is shown in Figure 5.11(a), where a noticeable reduction in the level of threshold voltage for the treated group has been recorded compared to the wild-type group. ΔV_T is nevertheless higher for the treated group with a concentration of 20 µg/mL than 125 µg/mL seen in Figure 5.8(a). Conversely, the data obtained from the OD600 measurement as illustrated in Figure 5.11(b) depict a contradictory image, the growth curves of both the treated group and the wild-type exhibit a high degree of similarity, suggesting a minimal differential impact of the treatment on the growth characteristics of the bacteria, and a minimal impact on bacterial cell density.
The observed mismatch in efficacy between the outcome of the electrical experiment and the OD600 measurements implies that the reduction in ΔV_T is attributed to metabolic factor, rather than change in proliferation or cell density, which is typically monitored by the OD600 measurement.
Based on the working mechanism of SiNWFET, a drop in the acidity of the aqueous solution is accompanied with a similar drop in threshold voltage of the transistors on the chip, that may occur when the metabolic overflow process is reversed due to an accelerated TCA cycle depriving the culture of its acidic molecules. Nevertheless, multiple studies have substantiated that the rate of oxygen consumption within a culture experiences a marked decline indicative of a receded respiration rate and a decelerated TCA cycle, upon the introduction of Chloramphenicol [52] [55]. Theoretically, in the treated group, the anticipated behavior of the metabolic process should lead to an increase in the threshold voltage level, contrary to the observed reduction. This expectation is based on the understanding that a lower activity in the TCA cycle is associated with an intensified overflow metabolism. Such an increase in overflow metabolism is expected to result in higher levels of acidic metabolites that could influence the pH level of the culture, thereby elevating the threshold voltage. The observed reduction in threshold voltage is, therefore, an atypical response from the bacterial culture.
The suggested explanation for this discrepancy between the theoretical knowledge and the empirical data entails, in addition to the inhibition of protein synthesis, the total inhibition of the metabolic process in the bacterial culture, including the overflow process from acetyl-CoA to acetate. Consequently, the acidic byproduct of the metabolic process will decline in contrast

to a healthy wild-type group, resulting in an elevated pH level and a lower threshold level in the tested silicon nanowire field-effect transistors.

Treatment with 250 µg/mL Chloramphenicol

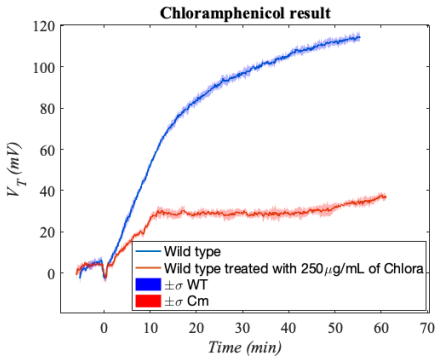

(a) ΔV_T vs time curve for 250 µg/mL of Chloramphenicol.

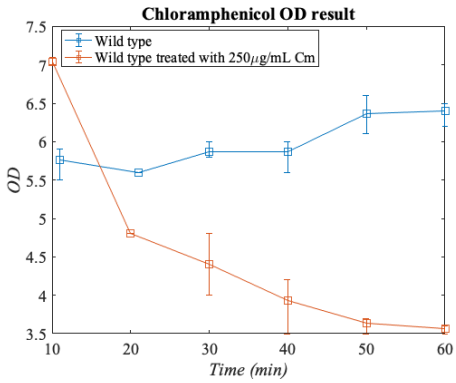

(b) OD results for 250 µg/mL of Chloramphenicol.

Figure 5.12: A comparison between the ΔV_T vs time curve and the OD measurements showing a discernible decrease in cell concentration with antibiotic concentration of 250 µg/mL..

The results from the electrical measurement as presented in Figure 5.12(a) suggest an amplification in the medium alkalization level that surpasses the last two examined concentrations. Although the slope of this line mirrors that of 125 µg/mL and 20 µg/mL in the first 10 minutes, however the slope experiences a sharp and sustained decrease unmatched by the recorded data for other concentrations.
The drop in ΔV_T is also reflected in the registered OD600 results plotted in Figure 5.12(b). The slope of the line subside drastically from the 10 to 20 minutes mark. Despite the OD600 readings for the concentration of 125 µg/mL of Chloramphenicol appearing lower than those for 250 µg/mL, when conducting a comprehensive analysis which take into consideration the initial baseline of both lines and the subsequent decline of each one, this will leads to the inference that the effective OD600 for the 250 µg/mL is lower than that of 125 µg/mL.
To explore the justification and source of the aforementioned decline in

OD600 measurements, a subsequent analysis using microfluidic device has been performed. This device consists an inlet, outlet and multiple trapping chambers which can capture bacterial cells and allows for test to be conducted in a non-invasive approach. To ensure the successful capture of cells inside the trapping chambers, the bacteria are introduced to the device via the inlet while blocking the outlet. Subsequently, the LB medium inside the device is renewed with fresh LB infused with antibiotic with the desired concentration. The device is placed under the microscope and a sample of bacteria is measured and quantified. Afterwards, the microfluidic chip is incubated on the hot plate at a temperature of 37 °C for 30 minutes. Post incubation the device is reexamined under the microscope to evaluate any variations in bacterial morphology and population density consequent to the antibiotic treatment.

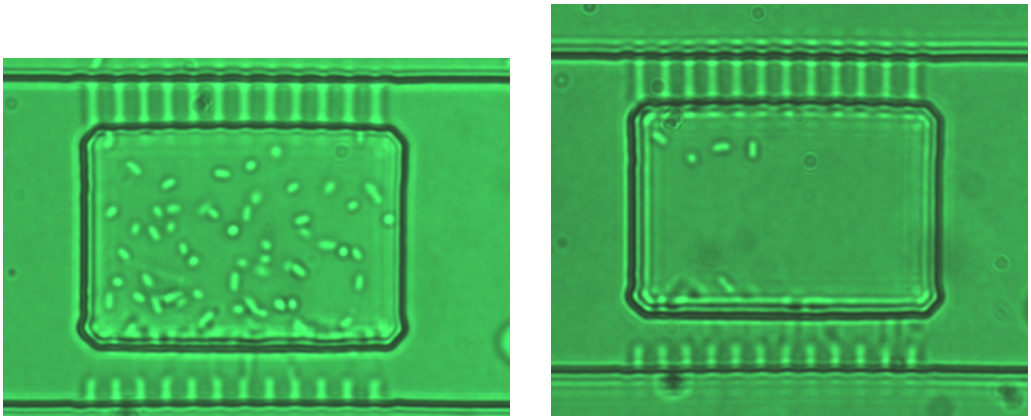

(a) Microscope image for wild-type.

(b) Microscope image for wild-type treated with Chloramphenicol.

Figure 5.13: Microscopic images of E. coli were captured both prior to the introduction of Chloramphenicol and 30 minutes post-addition of Chloramphenicol

Despite the finite range of resolution in the used microscope, and the limited number of bacteria trapped inside the trapping chamber, the resulting images, presented in Figure 5.13, indicate a deviation from the normal morphological form, as cells subjected to antibiotic treatment experienced a reduction in size. Population density was also negatively impacted by the the treatment.

To ascertain whether the observed decrement in cell count is attributed to the efficacy of antibiotic or to the egress of cells from the confinement of the trapping chambers, a new time kill assay was instituted, for which the results can be seen in Figure 5.14.

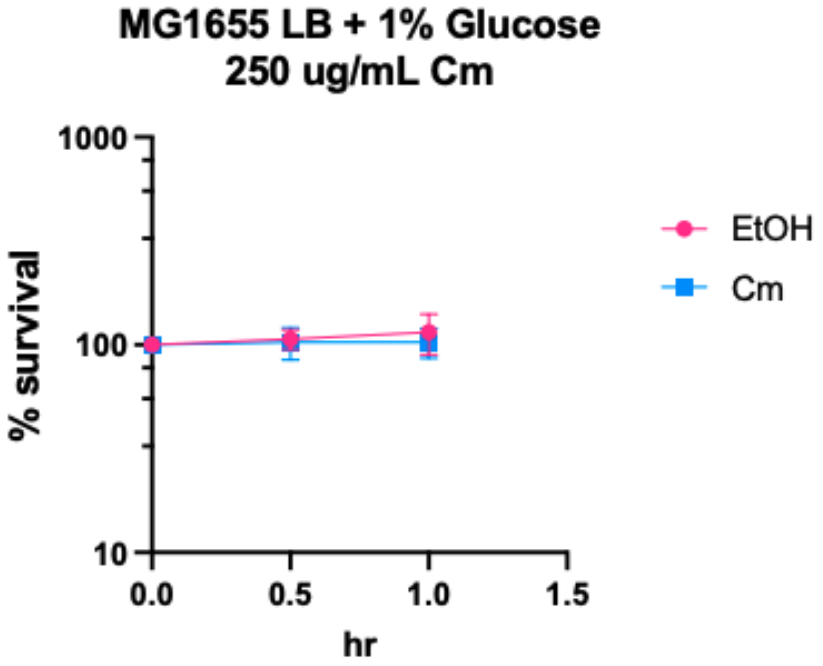

Figure 5.14: Results from the time kill assay conducted for 1 hour, using a concentration of 250 µg/mL.

Unsurprisingly, empirical data indicate that Chloramphenicol exhibits bacteriostatic characteristics at an elevated concentration of 250 µg/mL. This result suggests the reason for the sustained reduction in the OD600 measurement is attributed to inhibited overflow process and cell size which was negatively impacted by the treatment.
Regarding the electrical measurement results introduced in Figure 5.12(a), the substantial decrease observed in the threshold voltage is attributed to the bacteriostatic influence exerted by Chloramphenicol and the morphological alterations in the bacterial cells. To further elucidate, introducing bacteriostatic antibiotic to a bacterial culture inhibit protein syntheses and

as discussed earlier, the entire metabolic process including the overflow process from acetyl-CoA to acetate. Thereby the consequence of disrupting the metabolic process includes a decelerated extracellular acidification rate compared to the wild-type and a reduced threshold voltage of the SiNWFET. It is also responsible for the impaired growth observed under the microscope as the bacteria require the energy reserve molecule synthesized by metabolism such as ATP to conduct vital operations for growth such as cell wall, and proteins synthesis [56]. Additional source of basic molecules within the medium include cell cytoplasm which maintains a balanced pH level and can egress from the cell wall in response to the reduction in cell size, functioning as a compensatory mechanism to equilibrate osmotic pressure [57].

5.6 Challenges and solutions

Given the hardware-intensive nature of this project, software-related challenges were conspicuously absent from our observations. Predominantly, the encountered issues were oriented towards hardware and expertise complications and can be summarized as following:

- Inadequate knowledge in bacterial metabolism: Insufficient comprehension of bacterial metabolism posed challenges in explaining the experimental results. Mitigating this obstacle involved conducting an extended litterateur review to understand the process of the bacterial metabolism, and address this knowledge gap in that specific subject.

- Using the hardware: Most of the hardware, and machines in the clean room require proper training prior to utilization for research proposes. This step presented a challenge at the beginning of the project. However, a solution was implemented by engaging in a very short training course under the guidance of an experienced researcher. Subsequently, practical tasks were undertaken in their presence to reinforce the acquired skills.

- Drift in the signal: In order to obtain a reliable results, all the changes in the threshold voltage ΔV_T should originate from the bacterial culture. However, during multiple tests, we noticed an increase in threshold voltage before adding the bacteria. This drift in the signal was later attributed to an old reference electrode used to bias the transistor. This problem was solved temporarily by oxidizing the silver/silver-chloride

interface on the far end of the electrode, and permanently by purchasing a new reference electrode.

- Noisy and faulty signals: This problem is attributed to using an old batch of chip which has been repeatedly cleaned, biased and used to conduct the same experiment. The repeated cleaning and biasing of the chip create deficiencies in the hafnium oxide layer which works as the chip sensing layer. Solving this problem was achieved by fabricating new chips to be utilized in the experiment.

- Difficulties during the microfluidic test: During the execution of the microfluidic assays, several technical challenges were encountered that impeded optimal data acquisition, including the insufficient resolution of the microscope which proved inadequate for detailed observation of the bacterial specimens. Furthermore the dimension of the trapping chambers were large, permitting bacterial rotation and thereby complicating the precise quantification of cellular dimensions. Reaching a solution for these problems were not feasible in the time-frame of this project, as it requires a redesign of the microfluidic device, and acquiring a more powerful microscope to conduct the analysis.

Despite the above mentioned challenges, the experiment is very well repeated, and the results it provides are consistent and reliable.

6 Conclusions and future works

Due to the emergence of new resistant strains of bacteria, the fight against antimicrobial resistant is projected to accelerate in the next decade to circumvent the disastrous ramifications and protect human lives from the dangers posed by bacterial pathogens.
This project aims to aid the international scientific research in its endeavor against antibiotic resistance by introducing a novel technology capable of elucidating the alterations in bacterial metabolic processes and pathways induced by the introduction of antibiotics.
The results look promising as a clear deviation between threshold voltage line for the treated group and its wild-type counterpart is detected in most cases under the 30-minutes mark. This result paves the way for a fast, reliable AST with the potential to save thousands of lives.
Future works will include extending the experimental data to include various additional antibiotics, which will help create a data-base pertaining to how each of the tested antibiotics affects the bacteria and its metabolism. Other bacteria should also be tested in order to determine the efficacy of the antibiotics on the chosen bacteria, and aid health personnel in deciding the right antibiotic for any given pathogen.
Another area of interest include modifying the chip and the hardware to accommodate multiple test simultaneously, by including and integrating multiple transistors on the same chip for measuring the extracellular acidification rate, in addition to a fast and reliable switching unit and an accurate semiconductor parameter analyzer capable of handling the extra demand from the new devices. This step will substantially accelerate the experimental phase to ensure that the findings are duly documented and rendered accessible to healthcare professionals for analysis and further action.
Lastly, a suitable packaging for the chip, and a way to automate the test needs to be developed, in order to distribute the test kit to hospitals and health centers around the country. This step will establish the mean for doctors to use this chip for testing on their patients' specific pathogen rather than relying on the results from the generic test performed in our laboratories and determine the appropriate antibiotic and its dosage.

References

[1] C. L. Ventola, "The antibiotic resistance crisis: Part 1: Causes and threats," *Pharmacy and Therapeutics*, vol. 40, p. 277, 2015. [Online]. Available: /pmc/articles/PMC4378521/https://www.ncbi.nlm.nih.gov/pmc/articles/PMC4378521/

[2] H. C. Neu, "The crisis in antibiotic resistance," *Science*, vol. 257, no. 5073, pp. 1064–1073, 1992. [Online]. Available: https://www.science.org/doi/abs/10.1126/science.257.5073.1064

[3] P. Dadgostar, "Antimicrobial resistance: implications and costs," *Infection and Drug Resistance*, vol. 12, pp. 3903–3910, 2019. [Online]. Available: https://www.ncbi.nlm.nih.gov/pmc/articles/PMC6929930/

[4] M. Frieri, K. Kumar, and A. Boutin, "Antibiotic resistance," *Journal of Infection and Public Health*, vol. 10, pp. 369–378, 2017. [Online]. Available: http://dx.doi.org/10.1016/j.jiph.2016.08.007

[5] B. I. Coculescu, "Antimicrobial resistance induced by genetic changes," *Journal of Medicine and Life*, vol. 2, p. 114, 4 2009. [Online]. Available: /pmc/articles/PMC3018982//pmc/articles/PMC3018982/?report=abstracthttps://www.ncbi.nlm.nih.gov/pmc/articles/PMC3018982/

[6] C. Llor and L. Bjerrum, "Antimicrobial resistance: Risk associated with antibiotic overuse and initiatives to reduce the problem," *Therapeutic Advances in Drug Safety*, vol. 5, pp. 229–241, 2014. [Online]. Available: https://www.ncbi.nlm.nih.gov/pmc/articles/PMC4232501/

[7] Y. W. Tsai, T. C. Lin, H. Y. Chou, H. Y. Hung, C. K. Tan, L. C. Wu, I. J. Feng, and Y. L. Shiue, "Shortening the time of the identification and antimicrobial susceptibility testing on positive blood cultures with maldi-tof ms," *Diagnostics*, vol. 11, 8 2021. [Online]. Available: https://www.ncbi.nlm.nih.gov/pmc/articles/PMC8391154/

[8] J. Gao, J. Qin, C. Ding, Y. Gao, J. Guo, M. Li, C. Yang, and W. Wang, "Fluorescent metabolic labeling-based quick antibiotic susceptibility test for anaerobic bacteria," *RSC Chem. Biol.*, vol. 3, pp. 1314–1319, 2022. [Online]. Available: http://dx.doi.org/10.1039/D2CB00163B

[9] P. Swami, G. Verma, A. Holani, S. Kamaraju, V. Manchanda, V. Sritharan, and S. Gupta, "Rapid antimicrobial susceptibility profiling using impedance spectroscopy," *Biosensors and Bioelectronics*, vol. 200, p. 113876, 2022. [Online]. Available: https://www.sciencedirect.com/science/article/pii/S0956566321009131

[10] P. Woias, L. Meixner, and P. Fröstl, "Slow ph response effects of silicon nitride isfet sensors," *Sensors and Actuators B: Chemical*, vol. 48, pp. 501–504, 5 1998.

[11] M. Gotoh, S. Oda, I. Shimizu, A. Seki, E. Tamiya, and I. Karube, "Construction of amorphous silicon isfet," *Sensors and Actuators*, vol. 16, pp. 55–65, 1 1989.

[12] S. Zafar, C. D'Emic, A. Afzali, B. Fletcher, Y. Zhu, and T. Ning, "Optimization of ph sensing using silicon nanowire field effect transistors with hfo2 as the sensing surface," *Nanotechnology*, vol. 22, 10 2011, the use of HFO2 with SIO2 nano wire on the gate gives a great pH sensor that gets near Nernst level of 59mV/pH and is independent of the buffer concentration.

[13] P. Bergveld, "Thirty years of isfetology: What happened in the past 30 years and what may happen in the next 30 years," *Sensors and Actuators B: Chemical*, vol. 88, pp. 1–20, 1 2003.

[14] Q. Hu, "Silicon nanowire based electronic devices for sensing applications," 2023. [Online]. Available: http://urn.kb.se/resolve?urn=urn:nbn:se:uu:diva-439645

[15] N. Liu, R. Chen, and Q. Wan, "Recent advances in electric-double-layer transistors for bio-chemical sensing applications," *Sensors 2019, Vol. 19, Page 3425*, vol. 19, p. 3425, 8 2019. [Online]. Available: https://www.mdpi.com/1424-8220/19/15/3425/htmhttps://www.mdpi.com/1424-8220/19/15/3425

[16] J. Q. Li, L. Meng, and J. Cheng, "Thermodynamic conditions for the nernstian response of the flat band potential of the metal oxide semiconductor: A theoretical study," *Journal of Physical Chemistry C*, vol. 126, pp. 578–587, 1 2022. [Online]. Available: https://pubs.acs.org/doi/full/10.1021/acs.jpcc.1c07625

[17] F. Yang and G.-J. Zhang, "Silicon nanowire-transistor biosensor for study of molecule-molecule interactions," *Reviews in Analytical Chemistry*, vol. 33, 08 2014.

[18] K. I. Chen, B. R. Li, and Y. T. Chen, "Silicon nanowire field-effect transistor-based biosensors for biomedical diagnosis and cellular recording investigation," *Nano Today*, vol. 6, pp. 131–154, 4 2011.

[19] S. Baron, *Medical microbiology*. University of Texas Medical Branch at Galveston, 1996, ch. 4.

[20] "Metabolic pathways." [Online]. Available: https://www.genome.jp/pathway/map01100

[21] H. W. Doelle, *Bacterial metabolism*. Academic Press, 2014.

[22] P. Jurtshuk, *Bacterial metabolism*. University of Texas Medical Branch at Galveston, Texas, ed, 1996, vol. 4.

[23] T. Shimada, K. Nakazawa, T. Tachikawa, N. Saito, T. Niwa, H. Taguchi, and K. Tanaka, "Acetate overflow metabolism regulates a major metabolic shift after glucose depletion in escherichia coli," *FEBS letters*, vol. 595, pp. 2047–2056, 8 2021. [Online]. Available: https://pubmed.ncbi.nlm.nih.gov/34125966/

[24] Y. Anraku, "Bacterial electron transport chains," *https://doi.org/10.1146/annurev.bi.57.070188.000533*, vol. 57, pp. 101–132, 11 2003. [Online]. Available: https://www.annualreviews.org/doi/abs/10.1146/annurev.bi.57.070188.000533

[25] M. Ahmad, A. Wolberg, and C. I. Kahwaji, "Biochemistry, electron transport chain," *StatPearls*, 9 2022. [Online]. Available: https://www.ncbi.nlm.nih.gov/books/NBK526105/

[26] A. I. Jonckheere, J. A. Smeitink, and R. J. Rodenburg, "Mitochondrial atp synthase: architecture, function and pathology," *Journal of Inherited Metabolic Disease*, vol. 35, p. 211, 3 2012. [Online]. Available: /pmc/articles/PMC3278611//pmc/articles/PMC3278611/?report=abstracthttps://www.ncbi.nlm.nih.gov/pmc/articles/PMC3278611/

[27] K. Kita, C. R. Vibat, S. Meinhardt, J. R. Guest, and R. B. Gennis, "One-step purification from escherichia coli of complex ii (succinate: ubiquinone oxidoreductase) associated with succinate-reducible cytochrome b556." *The Journal of biological chemistry*, vol. 264, pp. 2672–2677, 2 1989. [Online]. Available: http://www.jbc.org/article/S0021925819816666/fulltexthttp://www.jbc.org/article/S0021925819816666/abstracthttps://www.jbc.org/article/S0021-9258(19)81666-6/abstract

[28] P. Iqbal, J. A. Preece, and P. M. Mendes, "Nanotechnology: The "top-down" and "bottom-up" approaches," *Supramolecular Chemistry*, 1 2012. [Online]. Available: https://onlinelibrary.wiley.com/doi/full/10.1002/9780470661345.smc195https://onlinelibrary.wiley.com/doi/abs/10.1002/9780470661345.smc195https://onlinelibrary.wiley.com/doi/10.1002/9780470661345.smc195

[29] K. L. Elbing and R. Brent, "Growth of e. coli in liquid medium," *Current protocols in molecular biology*, vol. 125, p. e81, 1 2019. [Online]. Available: /pmc/articles/PMC6375084//pmc/articles/PMC6375084/?report=abstracthttps://www.ncbi.nlm.nih.gov/pmc/articles/PMC6375084/

[30] B. Kowalska-Krochmal and R. Dudek-Wicher, "The minimum inhibitory concentration of antibiotics: Methods, interpretation, clinical relevance," *Pathogens*, vol. 10, pp. 1–21, 2 2021. [Online]. Available: /pmc/articles/PMC7913839//pmc/articles/PMC7913839/?report=abstracthttps://www.ncbi.nlm.nih.gov/pmc/articles/PMC7913839/

[31] J. Beal, N. G. Farny, T. Haddock-Angelli, V. Selvarajah, G. S. Baldwin, R. Buckley-Taylor, M. Gershater, D. Kiga, J. Marken, V. Sanchania, A. Sison, C. T. Workman, M. Pehlivan, B. B. Roige, T. Aarnio, S. Kivisto, J. Koski, L. Lehtonen, D. Pezzutto, P. Rautanen, W. Bian, Z. Hu, Z. Liu, Z. Liu, L. Ma, L. Pan, Z. Qin, H. Wang, X. Wang, H. Xu, X. Xu, Y. E. Moubayed, S. Dong, C. Fang, H. He, H. He, F. Huang, R. Shi, C. Tang, C. Tang, S. Xu, C. Yan, N. Bartzoka, E. Kanata, M. Kapsokefalou, X. L. Katopodi, E. Kostadima, I. V. Kostopoulos, S. Kotzastratis, A. E. Koutelidakis, V. Krokos, M. Litsa, I. Ntekas, P. Spatharas, O. E. Tsitsilonis, A. Zerva, V. Annem, E. Cone, N. Elias, S. Gupta, K. Lam, A. Tutuianu, D. M. Mishler, B. Toro,

A. Akinfenwa, F. Burns, H. Herbert, M. Jones, S. Laun, S. Morrison, Z. Smith, Z. Peng, Z. Ziwei, R. Deng, Y. Huang, T. Li, Y. Ma, Z. Shen, C. Wang, Y. Wang, T. Zhao, Y. Lang, Y. Liang, X. Wang, Y. Wu, D. Aizik, S. Angel, E. Farhi, N. Keidar, E. Oser, M. Pasi, J. Kalinowski, M. Otto, J. Ruhnau, H. Cubukcu, M. A. Hoskan, I. Senyuz, J. Chi, A. P. Sauter, M. F. Simona, S. Byun, S. Cho, G. Kim, Y. Lee, S. Lim, H. Yang, T. Xin, Z. Yaxi, P. Zhao, W. Han, F. He, Y. He, N. Li, X. Luo, C. Boxuan, H. Jiaqi, Y. Liangjian, L. Wanji, C. Xinguang, L. Xinyu, Z. Wu, Y. Xi, X. Yang, Y. Yang, Z. Yang, Y. Zhang, Y. Zhou, Y. Peng, L. Yadi, S. Yang, J. Yuanxu, K. Zhang, D. Abraham, T. Heger, C. Leach, K. Lorch, L. Luo, A. Gaudi, A. Ho, M. Huang, C. Kim, L. Kugathasan, K. Lam, C. Pan, A. Qi, C. Yan, K. Schaaf, C. Sillner, R. Coates, H. Elliott, E. Heath, E. McShane, G. Parry, A. Tariq, S. Thomas, C. W. Chen, Y. H. Cheng, C. W. Hsu, C. H. Liao, W. T. Liu, Y. C. Tang, Y. H. Tang, Z. E. Yang, L. Jian, C. Li, C. Lin, G. Ran, Z. Run, W. Ting, Z. Yong, L. Yu, A. C. Lind, A. Norberg, A. Olmin, J. Sjolin, A. Torell, C. Trivellin, F. Zorrilla, P. G. de Vries, H. Cheng, J. Peng, Z. Xiong, D. Altarawneh, S. S. Amir, S. Hassan, A. Vincent, B. Costa, I. Gallegos, M. Hale, M. Sonnier, K. Whalen, M. Elikan, S. Kim, J. You, R. Rambhatla, A. Viswanathan, H. Tian, H. Xu, W. Zhang, S. Zhou, L. Jiamiao, X. Jiaqi, D. Craw, M. Goetz, N. Rettedal, H. Yarbrough, C. Ahlgren, B. Guadagnino, J. Guenther, J. Huynh, Z. He, H. Liu, Y. Liu, M. Qu, L. Song, C. Yang, J. Yang, X. Yin, Y. Zhang, J. Zhou, L. Zi, Z. Jinyu, X. Kang, P. Xilei, H. Xue, S. Xun, P. Babu, A. Dogra, P. Thokachichu, D. Faurdal, J. H. Jensen, J. Mejlsted, L. Nielsen, T. Rasmussen, J. Denter, K. Husnatter, Y. Longo, J. C. Luzuriaga, E. Moncayo, N. T. Moreira, J. Tapia, T. Dingyue, Z. Jingjing, X. Wenhao, T. Xinyu, H. Xiujing, J. DeKloe, B. Astles, U. Baronaite, I. Grazulyte, M. Hwang, Y. Pang, M. A. Crone, R. Hosseini, M. Houmani, D. Zadeh, V. Zanotti, O. A. Baltensperger, E. Y. Bijman, E. Garulli, J. L. Krusemann, A. Martinelli, A. Martinez, T. Vornholt, M. Camille, A. Paul, E. Browne, D. B. J. Gilman, A. Hewitt, S. Hodson, I. Holmedal, F. Kennedy, J. Sackey, S. Beck, F. Eidloth, M. Imgold, A. Matheis, T. Meerbrei, D. Ruscher, M. Schaeftlein, Z. Hanrong, M. Wan, L. Dai, K. Jin, S. Wang, X. Wang, Y. Wang, Y. Wang, C. Wu, Z. Zhang, Y. Zhou, L. Xinyu, Z. Zirong, R. Babar, M. Brewer, C. Clodomir, L. D. Neves, A. Iwuogo, A. Jones, C. Jones, J. Kelly,

G. Kim, J. Siemer, Y. Yadav, Y. Ikagawa, T. Isogai, R. Niwa, C. Aubry, W. Briand, A. Jacq, S. Lautru, B. Marta, C. Maupu, X. Ollessa-Daragon, K. Papadopoulo, M. S. Azad, W. Kuangyi, Y. Xiu, C. Yang, A. Iyer, R. Prins, P. Yesley, F. Lichi, C. Z. Xuan, K. Jo, M. Park, S. Park, H. Yoo, N. Burckhardt, L. Daniels, B. Klopprogge, D. Kruger, O. E. Meyfarth, L. Putthoff, D. Wawrzyniak, X. Hu, Y. Wang, L. Badash, A. Baichman-Kass, A. Barshap, Y. Friedman, E. Milshtein, O. Vardi, S. Dong, Y. Gu, Y. Pei, R. Shi, F. Yang, J. Yang, X. Zhu, L. K. Ching, L. H. Ching, N. T. Chun, Y. M. Hin, L. T. Hong, C. W. Lam, Y. C. Lam, C. Matthew, C. T. Ngo, Y. Shuan, C. T. Wan, T. S. Yan, C. Y. Yee, T. C. Yu, Y. W. Yu, C. T. H. Anson, L. S. Choi, C. M. Chun, C. L. Hin, W. C. Hin, N. S. Ho, L. C. Y. Jay, L. M. W. Katherine, W. C. Kin-ning, L. H. Kiu, C. C. Kong, L. C. Wai, Y. W. Yan, W. T. Yeung, L. K. Yin, T. S. Y. Grace, L. K. C. Joe, N. T. C. Kenneth, C. M. Y. Shuan, F. Aldo, C. H. Pang, K. P. So, H. M. Wong, L. T. Ching, L. H. Ching, I. N. Fung, Y. S. Fung, L. C. Hong, H. O. Ning, J. C. H. Sang, Y. H. L. Elsa, C. Y. Hei, L. H. Sing, C. S. Wang, Y. Gu, Z. Rong, H. Song, P. Wang, Y. Wang, Y. Chen, H. Qiu, H. Ren, Z. Xiao, H. Heng, X. Rao, R. Tian, S. S. Deb, Y. L. Kamble, N. Kumbhojkar, B. Patel, S. Prakash, S. M. Reshamwala, P. Taskar, Gokul, A. B. Uday, A. Basu, R. Gandhi, J. Khaimani, A. Khenwar, S. Raut, T. Somvanshi, D. Das, S. Ghosh, H. Rai, N. M. Anand, A. K. Jainarayanan, P. Kalson, D. H. Liya, V. Mishra, S. S. Pai, M. Pitaliya, Y. Rana, R. Yadav, N. Arora, V. Arora, S. Jain, A. Patel, S. Sharma, P. Singh, A. Goenka, R. Jain, A. Jha, A. Kumar, A. Soni, S. Ananthakrishnan, V. Devi, M. Faidh, G. Jayaraman, M. S. Kittur, N. R. Mahapatra, S. Menon, A. B. Muthukrishnan, B. P. Kailash, B. Sabuwala, M. Shinde, S. Venkatraghavan, W. Liu, Z. Miao, T. Wang, Y. Wang, S. Zhang, R. Chai, Y. Ge, A. Hou, F. Liu, X. Liu, J. Mao, Z. Wang, H. Yu, H. Yuan, Y. Zhan, A. Ries, C. Wolfbeisz, T. Kanaya, Y. Kawasaki, T. Maruo, Y. Mori, T. Satoh, A. Chau, W. Y. Chu, A. Markiv, M. V. H. Marti, M. J. R. Medina, D. Raju, S. Sinha, Y. Choi, B. S. Ryu, G. Byagathvalli, E. Kim, M. Crooijmans, J. de Waard, C. van Amstel, A. Demchuk, T. Haight, D. J. Kim, A. Neda, L. Roberts, L. Saville, R. Takeyasu, D. Tobin, M. Akbary, R. Avileli, K. He, A. Pageni, L. Saville, D. D. Silva, N. D. Silva, K. Turton, M. Wu, A. Zhang, B. Chavez, P. Garavito, M. Latham, J. Ptak, D. Tharp, N. Izzati, M. Jonsson, N. Labecka,

S. Palo, R. Beale, D. Logel, A. E. Mellou, K. Myers, A. Alonso, R. H. Cifuentes, B. S. Clemente, G. S. Gonzalo, I. M. Hernandez, L. A. Hernandez, F. J. Q. Lombardero, D. Marquina, G. F. Rodriguez, I. A. Smet, T. Butterfield, E. Deshmukh-Reeves, N. Gogineni, S. Hemmings, I. Kabbara, I. Norvaisaite, R. Smith, D. Bauersachs, B. Daniel, R. Inckemann, A. Seiffermann, D. Stukenberg, C. Weile, V. Clerc, J. Ha, S. Totten, T. Chang, C. Jimenez, D. Maddiboina, B. L. Acar, E. Elcin, T. Inanc, G. Kantas, C. Kayihan, M. Secen, G. Suer, K. Ucan, T. Unal, M. Fischer, N. Jasti, T. Stewart, S. Caldwell, J. Lee, J. Schultz, T. C. Chang, P. H. Chen, Y. H. Cheng, Y. H. Hsu, C. yu Yeh, Z. Ding, Z. Li, S. Lockwood, K. Quinn, L. Carrillo, M. Heintze, L. Meneu, M. Peras, T. Yehouessi, K. Eilers, E. Falgenhauer, W. H. Kiu, J. Mayer, J. Mueller, S. von Schoenberg, D. Schwarz, B. Tunaj, Z. Hu, Y. Huang, Y. Li, C. Fang, J. Liu, Y. Liu, Y. Wu, S. Xu, L. Yuan, M. Edelmayer, M. Hiesinger, S. Hofer, B. Krainer, A. Oswald, D. Strasser, A. Zimmermann, Y. C. Chen, Y. Y. Chan, Y. C. Chang, N. R. Deng, C. Y. Ku, M. Z. Lee, H. Li, Z. Liu, G. Song, Y. Xiang, H. Yan, H. Huanying, J. Qiaochu, J. Shengjuan, P. Yujie, M. Burridge, K. Standforth, S. Went, L. Chenxi, W. Han, Z. Qipeng, L. Yifan, Q. Yiming, P. Yutong, S. Kou, L. Luan, U. Akova, L. Fitzgerald, B. Ikwuagwu, M. Johnson, J. Kurian, C. Throsberg, L. Allen, C. Humphreys, D. Partridge, M. Whittle, N. Zilinskaite, M. Lee, W. Lin, Y. Ma, K. Wang, H. Cheng, S. Chi, Y. C. Chuang, R. Huang, L. Y. Ko, Y. C. Lin, Y. Y. Tsai, C. C. Wang, K. C. Yu, H. N. Burud, C. Chen, A. K. Haralsvik, A. Marinovic, H. H. Pedersen, A. Sande, V. Solvang, S. K. Ming, A. Praditya, A. Abduraimova, A. Meirkhanova, A. Mukhanova, T. Mulikova, Y. Gou, C. Lu, J. Ma, C. Zhu, L. C. Y. Aaron, T. S. Iyer, W. Jiacheng, Y. P. Lim, B. T. X. Lin, A. Ramzeen, N. L. B. A. O. Yong, Y. T. S. Chua, Y. D. Fong, M. He, L. Y. Tan, Z. Jiahe, L. Mingge, L. Nianlong, L. Yueyi, C. Yuhan, A. Chang, C. C. Chen, R. Chou, J. Clapper, E. Lai, Y. Lin, K. Wang, J. Yang, M. Anwar, I. Chehade, I. Hariyani, S. Hau, A. Isaac, L. Karpauskaite, M. Magzoub, D. Obaji, Y. R. Song, Y. Yun, K. Sun, Y. Zhang, E. Beard, L. C. Crosby, N. Delalez, A. Karshenas, A. Kozhevnikov, J. Kryukova, K. Saini, J. Stocks, B. Sudarshan, M. Taylor, G. Wadhams, J. Windo, A. Ameziane, D. Bhatt, A. Casas, A. Levrier, A. Santos, N. E. M. Sia, E. Wintermute, A. Dejoux, D. Gopaul, L. Guerassimoff, S. Jaoui, M. Madelenat, S. Petracchini,

F. Cai, Y. Jianzhao, S. Shuyu, L. Tairan, L. Xin, L. Yongjie, H. Zhecheng, E. Becker, M. Greenwald, V. Hu, T. Pavelek, E. Pinto, Z. Wei, Z. Burgland, J. Chan, J. Dejoie, K. Fitzgerald, Z. Hartley, M. Rasheed, M. Schacht, M. Gahagan, E. Kelly, E. Krauss, Y. Cao, Y. Shen, X. Wang, H. Xu, J. Zhang, P. Chandramouli, A. J. A. F, S. Jayaraman, M. S. Jude, V. Kumar, H. Lekshmi, R. Preetha, K. Rashid, S. D. Kumar, B. S. M. Kumar, L. M. Barrat, J. S. Dissmann, J. Kalinowski, M. Otto, J. Ruhnau, F. Stuhlweissenburg, E. Ueding, A. Bohner, B. Clark, E. Deibel, L. Klaas, K. Pate, E. Weber, K. Cohen, A. Guseva, S. King, S. Yoon, S. Ambre, S. Bhowmick, N. Pange, K. Parab, V. Patel, M. Patil, A. Rajurkar, M. Rege, M. Sawant, S. Sawant, A. Vaidya, P. Ji, F. Luo, G. Ma, X. Xu, J. Yin, Y. Zhou, K. Zhu, Y. Huang, Y. Huang, J. Li, X. Li, H. Wang, K. Wang, W. Wang, X. Zhang, J. Zou, M. Bao, H. Kang, X. Liu, Y. Tao, Z. Wang, F. Yang, T. Zhang, Y. Zhong, J. Liu, J. Liu, L. Ma, X. Niu, L. Qian, L. Wang, Q. Yan, N. Zhao, W. Chen, Y. Zhou, J. Chen, J. Hao, Z. HuaYue, P. Li, Y. Pei, J. Qu, R. Wang, X. Wang, K. Wu, Y. Wu, M. Xiang, L. Yang, Z. Yang, L. Zhaoting, W. Fu, Z. Li, W. Tang, K. Zhang, H. Li, X. Shao, C. Yang, Y. Zeng, Y. Zhou, S. Dong, Y. Jung, S. R. Li, T. Li, J. Yu, S. Dong, T. Li, X. Miao, S. Wang, Y. Ding, J. Huang, Y. Li, T. Sun, Q. Tian, M. Wu, J. Xing, X. Xiong, Y. Yan, Q. Yihang, J. Zhang, Y. Zhou, Z. Zhou, Z. Chen, P. He, Y. Hong, C. Y. Hsiao, Z. Liang, Z. Liu, Y. Ran, S. Sun, R. Xia, D. Dong, W. Zhao, M. Hu, S. Hu, W. Shi, Shulun, H. Yan, Y. Ye, Y. Hong, Y. Pan, Y. Song, J. Zhang, Y. Zhao, D. Chater, A. Foda, Y. Li, U. Saade, V. Sayous, Y. Mo, W. Ren, C. Zeng, Y. Cao, C. Czekster, I. Dunstan, S. Powis, B. Reaney, E. Snaith, C. Young, E. Frankel, E. Glockner, I. Justice, S. Murugan, L. Penny, C. Garcia, S. Rentouli, P. Aggarwal, S. Budhan, W. Chiang, D. Kwasniak, K. Ledalla, M. Lee, N. Lo, M. Mullin, L. Y. Pan, J. Rakhimov, R. Ruzic, M. Shah, L. Velikov, S. Vincent, P. Horz, N. Kuebler, J. Notheisen, D. Doyle, J. Gu, W. Hu, S. Yang, T. Kehan, G. Menghan, M. Xiaowen, Y. Chen, Z. Kang, H. Ni, J. Chen, L. He, M. Luo, J. Tang, K. Boyce, J. Lee, M. Martin, J. V. Nguyen, L. Wan, A. Astapenka, T. Badalli, I. Borovko, N. Chulkova, I. Faustova, A. Kolosova, M. Loog, A. Maljavin, F. Matiyevskaya, V. Tuzov, C. Chang, R. Chou, J. Clapper, T. Ho, Y. D. Hsieh, E. Lai, L. Tsai, K. Wang, J. Wu, V. I. P. Dominguez, C. I. R. Fernandez,

D. O. Fierro, A. K. A. Nunez, J. P. R. Perez, M. L. Rivera, C. L. G. Trevizo, M. A. L. Velasco, C. J. C. Oropeza, A. F. H. Mendoza, J. A. J. Figueroa, L. M. Leal, S. A. P. Benavides, V. J. R. Martinez, A. L. R. Aguirre, A. B. S. Alvarado, M. S. C. Solano, N. E. T. Castillo, A. R. Zamora, E. de la Pena Thevenet, K. S. Blas, A. L. T. Huerta, A. C. Resendiz, F. Cruz, F. Diaz, D. Espinoza, A. C. Figueroa, A. C. Luque, R. Portillo, C. Senes, D. Tamayo, M. D. Toro, I. Alexopoulos, A. D. Giannopoulos, Y. Giannoula, G. Kyrpizidis, M. Xinyue, C. Xirui, S. Zhiwei, N. Adler, A. Caballero, C. Hamady, A. Ibrahim, J. Parmar, T. Rastogi, J. Yang, J. Delhomme, A. Henras, S. Heux, Y. Romeo, M. Toanen, C. Wagner, P. Zanoni, T. Lotz, E. Nickels, B. Suss, H. Warzecha, J. Zimmermann, E. Dubuc, B. Eijkens, S. Keij, S. Twisk, M. Verhagen, M. van den Oetelaar, A. Armstrong, N. Bennis, S. Bouwmeester, L. Buller, K. Kohabir, M. de Leeuw, V. Mangkusaputra, J. Mattens, J. Nijenhuis, T. Paez, L. Schmidtchen, G. van der Voort, G. Ge, X. Haoran, L. Xiaojin, E. Agena, E. Agena, S. Bath, R. Campbell, R. Dalangin, A. Kim, D. Sauvageau, I. Shkolnikov, D. Graves, J. Lang, J. Nieberding-Swanberg, A. Rao, A. Torres, A. Yao, A. Abbas, C. Luo, X. Zepeng, Z. Ziyi, J. Chen, C. Colgan, S. Dvorkin, R. Filzen, V. Patel, A. Scott, P. Zulueta, J. Acosta, L. Araya, F. Chavez, S. Farias, D. Garrido, A. Marcoleta, F. Munoz, P. Rivas, N. Colant, C. Fan, S. Frank, J. Gabrielli, P. Handal, V. Pinheiro, S. Santamaria, S. Withanage, F. Xue, A. Gerard, M. Lefevre, F. Milano, N. D. S. Oliveira, M. Parmentier, L. Rigon, E. Chamiec-Case, R. Chen, P. Crowley, S. Doyle, S. Kadimi, T. Vella, N. Adulyanukosol, T. A. Dusseaux, V. Forman, C. Hansen, S. Kofoed, S. Louis, M. R. Lykkegaard, D. Mancinotti, L. Meyer, S. Michelsen, M. Raadam, V. S. Rasmussen, E. A. Thormar, A. Uslu, N. leelahakorn, S. Ding, C. Li, H. Tan, Y. Xu, J. Yang, D. Gamoneda, N. Kantor, L. Trujillo-Rodriguez, M. Turner, S. George, K. McConnell, C. Pollitt, I. F. Amin, M. Ikhsan, V. V. Japranata, A. Laurentius, L. A. Nurachman, M. I. A. Pratama, Y. Dirven, L. Frohlich, D. Linke, V. Mertes, R. R. Rolfsnes, A. Saragliadis, S. Castillo, S. Chinnathambi, C. Ellermeier, J. Farrell, J. Fassler, E. Fuentes, S. Ryan, E. Sander, A. Bott, L. Healy, P. Karumanchi, A. Ruzicka, Z. Wang, G. Byatt, P. C. Despres, A. Dube, P. Lemieux, F. Lepetit, L. A. Lortie, F. D. Rouleau, S. Barrington, C. Basulto, S. Delgadillo, K. D. Leon, M. Madrid, C. Meas, A. Sabandal, M. A. Sanchez, J. Tsui,

N. Woodward, R. Battina, J. Boyer, A. Cherupalla, J. Chiang, M. Heng, C. Keating, T. Liang, C. K. Loke, J. Premo, K. Srinivasan, J. Starkel, D. Zheng, G. Astorino, R. V. Cott, J. Guo, D. Kortus, W. Niu, P. J. Freire, D. B. Pedrolli, N. V. Ribeiro, B. F. Silva, N. V. Vanini, M. S. da Mota, L. de Souza Crispim, T. Chapman, T. Gaitt, M. Jones, E. Watson, G. Lopez-Grado, L. Sans, M. Brink, V. Rajagopal, E. Ramstrom, A. Bete, Y. Camacho, J. Carter, C. Davis, J. Dong, A. Ehrenworth, M. Goodson, C. Guptil, M. Herrmann, C. Hung, H. Jesse, R. Krabacher, D. McDonald, P. Menart, T. O'Leary, L. Polanka, A. Poole, V. Varaljay, A. Appel, J. Cave, L. Huuki, M. McDonough, C. Mills, A. Mitropoulos, J. Pruneski, K. Wickiser, F. X. Buson, V. Flores, G. M. Lima, C. G. T. Rosa, G. Bao, H. Dong, Z. Luo, J. Peng, Y. An, C. Cheng, Z. Jiang, L. Kong, C. Luo, L. Luo, Y. Shi, E. Tang, P. Wang, Y. Wang, G. Xu, W. Yu, B. Zhang, Q. Zhang, D. Garcia, N. Jiang, B. Kristy, R. Laurel, K. Leitner, F. Loeffler, S. Ripp, M. Street, K. Amheine, F. Bindt, M. Boer, M. Boxem, J. Govers, S. Jongkees, L. Pattiradjawane, P. Swart, H. Tsang, F. de Graaf, M. ten Dam, F. van Heijningen, Y. Boada, A. Vignoni, V. Brasas, A. Gaizauskaite, G. Jakutis, S. Jasiunas, I. Juskaite, J. Ritmejeris, D. Vaitkus, T. Venclovas, K. Vitkute, H. Yeliseyeva, K. Zukauskaite, J. Zvirblyte, L. Karpus, I. Mazelis, I. Rokaitis, N. D. Akingbesote, D. Culfogienis, W. Huang, K. Park, J. Ahuja, C. Corre, G. Dhaliwal, R. Evans, K. Hill, O. Holman, A. Jaramillo, A. Khalid, J. Lawrence, L. Mansfield, J. O'Brien, J. Ong, S. Prakash, J. Whiteside, K. Anderson, E. Chun, G. Kim, A. Nguyen, C. Shola, D. Toghani, A. Wong, J. Wong, J. Yung, E. Johnson, D. Lahad, K. Nicholson, H. Pedamallu, C. Phelan, C. Fikry, L. Fulton, N. Lassel, D. Perera, M. Robin, N. Shaw, K. Bowman, S. Coleman, K. Emilov, C. Gaspar, J. Jenakendran, S. Mubeen, M. Obrvan, C. Smith, T. Bo, D. Liaoqi, C. Tianyi, X. Yuan, Q. Yue, S. Do, X. Fang, E. Jones, J. Laury, W. Liu, A. Oliver, L. Parr, M. Saha, C. Shen, T. Son, J. Urban, Y. Verma, H. Zhou, S. Dong, Z. Hao, Y. Kuang, T. Liu, R. Zhou, B. Arruda, N. Farny, M. Hao, C. Pearce, A. Rebello, A. Sharma, K. Sumner, B. Sweet, J. Lin, D. Mengtao, F. Peiyao, F. Xinlei, N. Cai, J. Chen, Y. Fu, Y. Hu, Y. Qiang, Q. Wang, R. Yang, C. Yucheng, J. Zheng, K. Chang, C. Gao, F. Isaacs, K. Li, R. Moscoso, J. Patel, L. Telesz, A. Tirad, Q. Cao, X. Feng, Y. Lu, X. Zhang, X. Zhou, D. Sun, Z. Yuan, and J. Zhou,

"Robust estimation of bacterial cell count from optical density," *Communications Biology 2020 3:1*, vol. 3, pp. 1–29, 9 2020. [Online]. Available: https://www.nature.com/articles/s42003-020-01127-5

[32] M. Li, Q. Liu, Y. Teng, L. Ou, Y. Xi, S. Chen, and G. Duan, "The resistance mechanism of escherichia coli induced by ampicillin in laboratory," *Infection and Drug Resistance*, vol. 12, p. 2853, 2019. [Online]. Available: /pmc/articles/PMC6750165//pmc/articles/PMC6750165/?report=abstracthttps://www.ncbi.nlm.nih.gov/pmc/articles/PMC6750165/

[33] P. Belenky, J. D. Ye, C. B. Porter, N. R. Cohen, M. A. Lobritz, T. Ferrante, S. Jain, B. J. Korry, E. G. Schwarz, G. C. Walker, and J. J. Collins, "Bactericidal antibiotics induce toxic metabolic perturbations that lead to cellular damage," *Cell reports*, vol. 13, pp. 968–980, 11 2015. [Online]. Available: https://pubmed.ncbi.nlm.nih.gov/26565910/

[34] J. Lemire, A. Alhasawi, V. P. Appanna, S. Tharmalingam, and V. D. Appanna, "Metabolic defence against oxidative stress: the road less travelled so far," *Journal of applied microbiology*, vol. 123, pp. 798–809, 10 2017. [Online]. Available: https://pubmed.ncbi.nlm.nih.gov/28609580/

[35] M. A. Lobritz, P. Belenky, C. B. Porter, A. Gutierrez, J. H. Yang, E. G. Schwarz, D. J. Dwyer, A. S. Khalil, and J. J. Collins, "Antibiotic efficacy is linked to bacterial cellular respiration," *Proceedings of the National Academy of Sciences of the United States of America*, vol. 112, pp. 8173–8180, 7 2015. [Online]. Available: https://www.pnas.org/doi/abs/10.1073/pnas.1509743112

[36] K. T. Fitzgerald and K. L. Newquist, "Poisonings in the captive reptile," *Small Animal Toxicology, Third Edition*, pp. 229–249, 1 2013.

[37] J. Sojo-Dorado and J. Rodríguez-Baño, "Gentamicin," *Kucers the Use of Antibiotics: A Clinical Review of Antibacterial, Antifungal, Antiparasitic, and Antiviral Drugs, Seventh Edition*, pp. 964–991, 4 2023. [Online]. Available: https://www.ncbi.nlm.nih.gov/books/NBK557550/

[38] B. Plitzko and S. Loesgen, "Measurement of oxygen consumption rate (ocr) and extracellular acidification rate

(ecar) in culture cells for assessment of the energy metabolism," *Bio-protocol*, vol. 8, 5 2018. [Online]. Available: /pmc/articles/PMC8275291//pmc/articles/PMC8275291/?report=abstracthttps://www.ncbi.nlm.nih.gov/pmc/articles/PMC8275291/

[39] "Fluoroquinolones," *LiverTox: Clinical and Research Information on Drug-Induced Liver Injury*, 3 2020. [Online]. Available: https://www.ncbi.nlm.nih.gov/books/NBK547840/http://www.pubmedcentral.nih.gov/articlerender.fcgi?artid=PMC3992250

[40] T. Thai, B. H. Salisbury, and P. M. Zito, "Ciprofloxacin," *StatPearls*, 8 2023. [Online]. Available: https://www.ncbi.nlm.nih.gov/books/NBK535454/http://www.pubmedcentral.nih.gov/articlerender.fcgi?artid=PMC5727987

[41] M. Goswami, S. H. Mangoli, and N. Jawali, "Involvement of reactive oxygen species in the action of ciprofloxacin against escherichia coli," *Antimicrobial Agents and Chemotherapy*, vol. 50, pp. 949 – 954, 3 2006.

[42] D. J. Dwyer, M. A. Kohanski, B. Hayete, and J. J. Collins, "Gyrase inhibitors induce an oxidative damage cellular death pathway in escherichia coli," *Molecular Systems Biology*, vol. 3, p. 91, 1 2007.

[43] C. S. Lewin, I. Morrissey, and J. T. Smith, "The mode of action of quinolones: The paradox in activity of low and high concentrations and activity in the anaerobic environment," *European Journal of Clinical Microbiology Infectious Diseases*, vol. 10, pp. 240 – 248, 4 1991.

[44] G. V. Smirnova, A. V. Tyulenev, N. G. Muzyka, M. A. Peters, and O. N. Oktyabrsky, "Ciprofloxacin provokes sos-dependent changes in respiration and membrane potential and causes alterations in the redox status of escherichia coli," *Research in microbiology*, vol. 168, pp. 64–73, 1 2017. [Online]. Available: https://pubmed.ncbi.nlm.nih.gov/27498196/

[45] G. Smirnova, A. Tyulenev, N. Muzyka, V. Ushakov, Z. Samoilova, and O. Oktyabrsky, "Influence of growth medium composition on physiological responses of escherichia coli to the action of chloramphenicol and ciprofloxacin," *BioTech*, vol. 12, 6 2023. [Online]. Available:

/pmc/articles/PMC10296315//pmc/articles/PMC10296315/?report=abstracthttps://www.ncbi.nlm.nih.gov/pmc/articles/PMC10296315/

[46] G. P. Dinos, C. M. Athanassopoulos, D. A. Missiri, P. C. Giannopoulou, I. A. Vlachogiannis, G. E. Papadopoulos, D. Papaioannou, and D. L. Kalpaxis, "Chloramphenicol derivatives as antibacterial and anticancer agents: Historic problems and current solutions," *Antibiotics*, vol. 5, 6 2016. [Online]. Available: /pmc/articles/PMC4929435//pmc/articles/PMC4929435/?report=abstracthttps://www.ncbi.nlm.nih.gov/pmc/articles/PMC4929435/

[47] N. Patil and P. Mule, "Sensitivity pattern of salmonella typhi and paratyphi a isolates to chloramphenicol and other anti-typhoid drugs: An in vitro study," *Infection and Drug Resistance*, vol. 12, p. 3217, 2019. [Online]. Available: /pmc/articles/PMC6800285//pmc/articles/PMC6800285/?report=abstracthttps://www.ncbi.nlm.nih.gov/pmc/articles/PMC6800285/

[48] I. Nagao, "Comparative study of roseomycin, streptomycin, chloramphenicol and homosulfanilamide on the effect of experimental cholera infections," *The Tohoku journal of experimental medicine*, vol. 58, pp. 191–194, 1953. [Online]. Available: https://pubmed.ncbi.nlm.nih.gov/13136153/

[49] E. Scholar, "Chloramphenicol," *xPharm: The Comprehensive Pharmacology Reference*, pp. 1–7, 1 2007.

[50] B. Sanga and M. K. Kharel, "Chloramphenicol," *Encyclopedia of Toxicology*, pp. 825–830, 1 2024. [Online]. Available: https://linkinghub.elsevier.com/retrieve/pii/B9780128243152003493

[51] A. Sauerbrei, "Bactericidal and virucidal activity of ethanol and povidone-iodine," *MicrobiologyOpen*, vol. 9, 9 2020. [Online]. Available: /pmc/articles/PMC7520996//pmc/articles/PMC7520996/?report=abstracthttps://www.ncbi.nlm.nih.gov/pmc/articles/PMC7520996/

[52] D. J. Dwyer, P. A. Belenky, J. H. Yang, I. C. MacDonald, J. D. Martell, N. Takahashi, C. T. Chan, M. A. Lobritz, D. Braff, E. G. Schwarz, J. D. Ye, M. Pati, M. Vercruysse, P. S. Ralifo, K. R. Allison, A. S. Khalil, A. Y. Ting, G. C. Walker, and J. J. Collins, "Antibiotics

induce redox-related physiological alterations as part of their lethality," *Proceedings of the National Academy of Sciences of the United States of America*, vol. 111, pp. E2100–E2109, 5 2014. [Online]. Available: https://www.pnas.org/doi/abs/10.1073/pnas.1401876111

[53] J. L. ALLISON, R. E. HARTMAN, R. S. HARTMAN, A. D. WOLFE, J. CIAK, and F. E. HAHN, "Mode of action of chloramphenicol vii," *Journal of Bacteriology*, vol. 83, pp. 609–615, 1962. [Online]. Available: https://journals.asm.org/doi/10.1128/jb.83.3.609-615.1962

[54] R. B. Morrison, S. E. Bagoury, and S. Fletcher, "Effect of chloramphenicol in maintaining the viability of escherichia coli," *Nature 1956 178:4548*, vol. 178, pp. 1467–1467, 1956. [Online]. Available: https://www.nature.com/articles/1781467a0

[55] C. Wisseman Jr, J. Smadel, F. Hahn, and H. Hopps, "Mode of action of chloramphenicol i: Action of chloramphenicol on assimilation of ammonia and on synthesis of proteins and nucleic acids in escherichia coli," *Journal of bacteriology*, vol. 67, no. 6, pp. 662–673, 1954.

[56] A. G. Marr, "Growth rate of escherichia coli," *Microbiological Reviews*, vol. 55, no. 2, pp. 316–333, 1991. [Online]. Available: https://journals.asm.org/doi/abs/10.1128/mr.55.2.316-333.1991

[57] B. Poolman, "Physicochemical homeostasis in bacteria," *FEMS Microbiology Reviews*, vol. 47, pp. 1–7, 7 2023. [Online]. Available: https://dx.doi.org/10.1093/femsre/fuad033